การพัฒนาแพลเลเดียม-คอปเปอร์อัลลอยด์เมมเบรนที่ต้านทานต่อไฮโดรเจนเอมบริตเทิลเมนต์

นางสาวรัชนีกร ชูเกียรติไทย

วิทยานิพนธ์นี้เป็นส่วนหนึ่งของการศึกษาตามหลักสูตรปริญญาวิทยาศาสตรมหาบัณฑิต
สาขาวิชาปิโตรเคมีและวิทยาศาสตร์พอลิเมอร์
คณะวิทยาศาสตร์ จุฬาลงกรณ์มหาวิทยาลัย
ปีการศึกษา 2560

DEVELOPMENT OF HYDROGEN EMBRITTLEMENT RESISTED Pd-Cu ALLOY MEMBRANE

Miss Ratchaneekorn Chukiatthai

A Thesis Submitted in Partial Fulfillment of the Requirements
for the Degree of Master of Science Program in Petrochemistry and Polymer Science
Faculty of Science
Chulalongkorn University
Academic Year 2017

Thesis Title	DEVELOPMENT OF HYDROGEN EMBRITTLEMENT RESISTED Pd-Cu ALLOY MEMBRANE
By	Miss Ratchaneekorn Chukiatthai
Field of Study	Petrochemistry and Polymer Science
Thesis Advisor	Assistant ProfessorSukkaneste Tungasmita, Ph.D.
Thesis Co-Advisor	ProfessorSupawan Tantayanon, Ph.D.

Accepted by the Faculty of Science, Chulalongkorn University in Partial Fulfillment of the Requirements for the Master's Degree

.....Dean of the Faculty of Science
(Associate ProfessorPolkit Sangvanich, Ph.D.)

THESIS COMMITTEE

.....Chairman
(Assistant ProfessorBoonchoat Paosawatyanyong, Ph.D.)

.....Thesis Advisor
(Assistant ProfessorSukkaneste Tungasmita, Ph.D.)

.....Thesis Co-Advisor
(ProfessorSupawan Tantayanon, Ph.D.)

.....Examiner
(Prasit Pattananuwat, Ph.D.)

.....External Examiner
(Sutheerawat Samingprai, Ph.D.)

รัชนีกร ชูเกียรติไทย : การพัฒนาแพลเลเดียม-คอปเปอร์อัลลอยด์เมมเบรนที่ต้านทานต่อไฮโดรเจนเอมบริตเทิลเมนต์ (DEVELOPMENT OF HYDROGEN EMBRITTLEMENT RESISTED Pd-Cu ALLOY MEMBRANE) อ.ที่ปรึกษาวิทยานิพนธ์หลัก: ผศ. ดร.สุคคเณศ ตุงคะสมิต, อ.ที่ปรึกษาวิทยานิพนธ์ร่วม: ศ. ดร. ศุภวรรณ ตันตยานนท์, หน้า.

การพัฒนาแพลเลเดียม–คอปเปอร์อัลลอยด์เมมเบรนสำหรับการแยกก๊าซไฮโดรเจนที่อุณหภูมิต่ำกว่า 300 องศาเซลเซียสโดยปราศจากปัญหาไฮโดรเจนเอมบริตเทิลเมนต์นั้น เป็นที่น่าสนใจสำหรับอุตสาหกรรมปิโตรเคมี แพลเลเดียม–คอปเปอร์เมมเบรนถูกเตรียมขึ้นด้วยวิธีการเคลือบที่ไม่ใช้ไฟฟ้าและการเคลือบที่ใช้ไฟฟ้าบนตัวรองรับเหล็กกล้าไร้สนิม โดยที่องค์ประกอบของแพลเลเดียม–คอปเปอร์อัลลอยด์เมมเบรนมีความสัมพันธ์กับอัตราการการเคลือบของโลหะทั้งสอง โดยสภาวะที่เหมาะสมสำหรับการอบแพลเลเดียม–คอปเปอร์เมมเบรนเพื่อให้อยู่ในรูปอัลลอยด์ที่สมบูรณ์นั้นคือ 500 องศาเซลเซียสในบรรยากาศอาร์กอนเป็นเวลา 24 ชั่วโมง พบว่าหลังการอบแพลเลเดียม–คอปเปอร์เมมเบรนที่สภาวะดังกล่าวนั้นอะตอมของคอปเปอร์มีการกระจายตัวไปยังแพลเลเดียมอัลลอยด์เมมเบรน สำหรับลักษณะพื้นผิว องค์ประกอบ และโครงสร้างผลึกของแพลเลเดียม–คอปเปอร์อัลลอยด์เมมเบรน ได้ตรวจสอบโดยใช้กล้องจุลทรรศน์แบบส่องกราดที่ติดตั้งเครื่องวิเคราะห์เชิงพลังงาน (อีดีเอ็กซ์) และเครื่องวัดการเลี้ยวเบนรังสีเอ็กซ์ (เอ็กซ์อาร์ดี) พบว่าองค์ประกอบที่ดีที่สุดของแพลเลเดียมในแพลเลเดียม–คอปเปอร์อัลลอยด์เมมเบรนคือ 84 และ 75 เปอร์เซ็นต์ ปริมาณการแพร่ผ่านของไฮโดรเจนวัดที่อุณหภูมิ 150–300 องศาเซลเซียสและความแตกต่างของความดัน 0.5–2.5 บาร์ พบว่าปริมาณการแพร่ผ่านของก๊าซไฮโดรเจนเพิ่มขึ้นเมื่ออุณหภูมิและความดันเพิ่มขึ้น ดังนั้นการเติมคอปเปอร์ไปในแพลเลเดียมเมมเบรนมีส่วนช่วยในการลดความเครียดภายในโครงสร้างของแพลเดียมจึงส่งผลต่อความต้านทานไฮโดรเจนเอมบริตเทิลเมนต์ที่ทำให้แพลเลเดียม–คอปเปอร์อัลลอยด์เมมเบรนสามารถใช้งานที่อุณหภูมิต่ำกว่าอุณหภูมิวิกฤตของแพลเดียมเมมเบรนโดยปราศจากการเปราะเนื่องด้วยก๊าซไฮโดรเจน

สาขาวิชา ปิโตรเคมีและวิทยาศาสตร์พอลิเมอร์ ลายมือชื่อนิสิต .....

ปีการศึกษา 2560 ลายมือชื่อ อ.ที่ปรึกษาหลัก .....

ลายมือชื่อ อ.ที่ปรึกษาร่วม .....

5872033723 : MAJOR PETROCHEMISTRY AND POLYMER SCIENCE
KEYWORDS: PALLADIUM-COPPER ALLOY MEMBRANE, HYDROGEN EMBRITTLEMENT

RATCHANEEKORN CHUKIATTHAI: DEVELOPMENT OF HYDROGEN EMBRITTLEMENT RESISTED Pd-Cu ALLOY MEMBRANE. ADVISOR: ASST. PROF.SUKKANESTE TUNGASMITA, Ph.D., CO-ADVISOR: PROF.SUPAWAN TANTAYANON, Ph.D., pp.

The development of PdCu alloy membranes that can be used in hydrogen separation at low working temperature (<300°C) without hydrogen embrittlement problem is a very attractive topic for the petrochemical industry. Pd–Cu membranes have been prepared by electroless plating and electroplating method on stainless steel support. The compositions of the PdCu alloy membranes were related to both the metal deposition rates. The appropriate annealing temperature of Pd–Cu membranes was found at 500 °C in argon atmosphere for 24 hours to form a complete alloy material. After thermal annealing, the Cu atom was distributed in Pd alloy membrane. The surface morphology, compositions, and crystallinity of the PdCu alloy membranes were characterized using scanning electron microscopy (SEM), energy-dispersive X-ray spectroscopy (EDS) and X-ray diffraction (XRD). The best Pd contents in PdCu alloy membrane were about 84 and 75 %at. The hydrogen flux through the PdCu alloy membrane was measured at temperature 150 to 300 °C and differential pressure 0.5 to 2.5 bar for membrane stability. The hydrogen flux increased with increasing temperature and pressure. Adding Cu atoms in Pd can reduce strain in Pd lattice structure. Both PdCu alloy membrane can be operated at the lower temperature than a critical temperature of pure Pd membrane without hydrogen embrittlement.

Field of Study:	Petrochemistry and Polymer Science	Student's Signature	.....
		Advisor's Signature	.....
Academic Year:	2017	Co-Advisor's Signature	.....

ACKNOWLEDGEMENTS

I would like to express my sincere thankfulness and appreciation to my advisor, Assistant Professor Dr. Sukkanest Tungasmita, who has been abundantly helpful guidance and encouragement throughout education at Chulalongkorn University. I also would like to especially thank my co-adviser. Professor Dr. supawan Tantayanon, who helped and gave wealth of information and input has been proved invaluable to this research project. Moreover, I would like to thank my committee members, Assistant Professor Dr. Boonchoat Paosawatyanyong, Dr. Prasit Pattananuwat and external examiner Dr. Sutheerawat Samingprai. In addition, I also would like to thank Dr. Duangamol Tungasmita for guidance throughout this work.

I would like to extend my deepest gratitude to Dr. Sarocha Sumrunronnasak and Dr. Maslin Chotirat for teaching and guidance throughout this work. I gratefully acknowledge the supports from PTT Global Chemical Public Company Limited and PTT Research and Technology Institute

Last but not least; I would like to thank my parents, my sister, my friend and my family for all the love, trust, support and understanding. Their encouragement is greatly acknowledged.

CONTENTS

Page

CONTENT OF FIGURE

LIST OF TABLES

CHAPTER I

INTRODUCTION

1.1 Introduction

Hydrogen has been interested in a few decades because it can be used as the renewable resource. In the chemical industrial process, hydrogen is well known to be use for the production of ammonia gas in fertilizer and also be utilized for some particularly chemical processes such as hydrogen cracking, hydrogen alkylation and hydrodesulfurization [1]. The demand for high purity hydrogen (99.999 %) is increasing very rapid and need some special technologies for the hydrogen separation such as pressure swing adsorption, cryogenic recovery and membrane separation. The membrane separation technology has been the most interesting because of reducing cost of operation and low energy requirement [2].

Pd based membrane have the innate ability for hydrogen separation due to high selectivity and high permeation. Hydrogen molecule can dissociate on the surface of Pd to form hydrogen atoms and no other gas molecule can pass to the Pd or Pd-alloy films [3]. A problem of Pd membrane is that the absorption of hydrogen below its critical temperature of 300°C and 2 MPa causes two different phases (α and β) as shown Figure 1.1, both of which maintain the face-center cubic (f.c.c.) crystal structure. The crystal unit cell lattice parameter (***a***) is increased from 3.890 Å for palladium to 3.895 Å for α phase and up to 0.4100 Å for β phase. The phase transformation (α to β) can occur with a lattice volume expansion in excess of 10% [4]. This occurs due to the difference between the α and β phase are created internal strain. This strain can lead to

the distortion in membrane crystal structure. Hydrogen absorption/desorption cycles at room temperature, the α to β and β to α transitions will occur to the deformation or cracking of the Pd membrane. This phenomenon, called 'hydrogen embrittlement' [5].

Elemental	Lattice parameter (*a*) Å
Pd	3.890
Pd-H in α phase	3.895
Pd-H in β phase	4.100

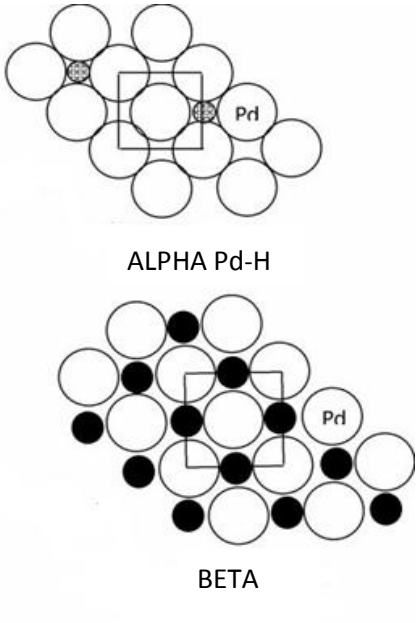

Figure 1.1 Image of alpha phase and beta phase[6]

Hydrogen embrittlement is the result of the exposure hydrogen in metals which caused to the loss of ductility in metal [6]. To prevent phase transition, alloying of Pd with other metallic element such as Cu, Au, Ag, Fe, Ni and Y can help decreasing the critical temperature of Pd membrane. Pd alloy membranes can be use in hydrogen absorption/desorption cycles at lower temperatures than 300°C without hydrogen embrittlement [7-10].

In this work, PdCu alloy membranes were prepared on porous stainless steel supports by electroless plating and electroplating methods. The alloying was done by

diffusion process via thermal annealing to form PdCu alloy. The physical characteristics of the membranes were investigated by using X–ray diffraction (XRD), scanning electron microscopy (SEM) and energy dispersive X–ray spectroscopy (EDS) techniques. The hydrogen performance of PdCu alloy membranes were measured at temperature 150–300 °C and differential pressure (ΔP) from 0.5 to 2.5 bar and hydrogen embrittlement test showed that the PdCu alloy membrane can be operated at much lower temperature than critical temperature of Pd membrane without micro-crack.

1.2 Objective

The aim of this work is to prepare PdCu alloy membrane, which can be operated at much lower temperature than critical temperature of Pd membrane, without failure hydrogen embrittlement.

1.3 Scope of research

1. To prepare and characterize PdCu alloy membranes which are formed completely in alloy on porous stainless steel support.
2. To study the stability of PdCu alloy membranes at low working temperature without hydrogen embrittlement.

CHAPTER II

THEOTY AND LITTERETURE REVIEW

2.1 Palladium membrane for hydrogen separation

Palladium is a transition metal of group 10 in the periodic table. The density of palladium is 12.023 g/cm^3 with the melting point at 1555.05 °C. Palladium has the face-center cubic (f.c.c.) crystal structure with lattice parameter of 3.890 Å [4]. As thin layer, the dense palladium layer membrane has the ability to separate only hydrogen from the mixture of gases as in Figure 2.1. The high-pressure side of Pd layer membrane is called feed side while the low-pressure side is called permeation side [11]. The mass transfer may occur under a variety of driving forces such as gradient of concentration, pressure, temperature, electric potential [12].

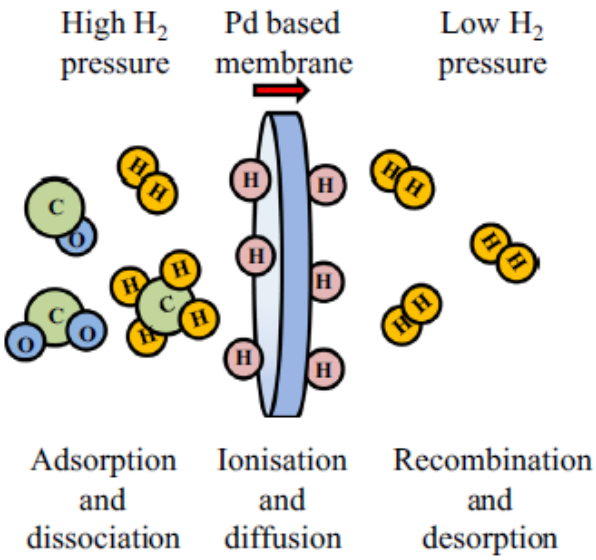

Figure 2. 1 Schematic of hydrogen separation from the mixture of gases [12]

2.1.1 Mechanism and properties of palladium membrane

The Pd membrane has the ability to dissociate molecular hydrogen into monatomic hydrogen for fast diffusion process in hydrogen separation. Normally, free Pd atom has an outer electron configuration of $1s^2\ 2s^2\ 2p^6\ 3s^2\ 3p^6\ 3d^{10}\ 4s^2\ 4p^6\ 4d^{10}\ 5s^0$. There is an overlapping energy bands between the 4d and 5s which is typical of transition metals. This gives Pd a high affinity for donor electrons from other atoms, which is unique ability to permeate hydrogen of Pd [12].

The mechanism of palladium membrane is well known collectively as solution–diffusion mechanism. The mechanisms of hydrogen transport from high-pressure to low-pressure were shown in Figure 2.2 [13]. The step can be explained, as following:

1. In the first step, adsorption of molecular hydrogen on the surface membrane
2. Dissociation of molecular hydrogen into atom on the surface
3. Dissolution of atomic hydrogen into the bulk metal
4. Diffusion of the hydrogen atom through the bulk membrane
5. Recombination of hydrogen atoms to form hydrogen molecules on the surface
6. Desorption of molecular hydrogen from the surface

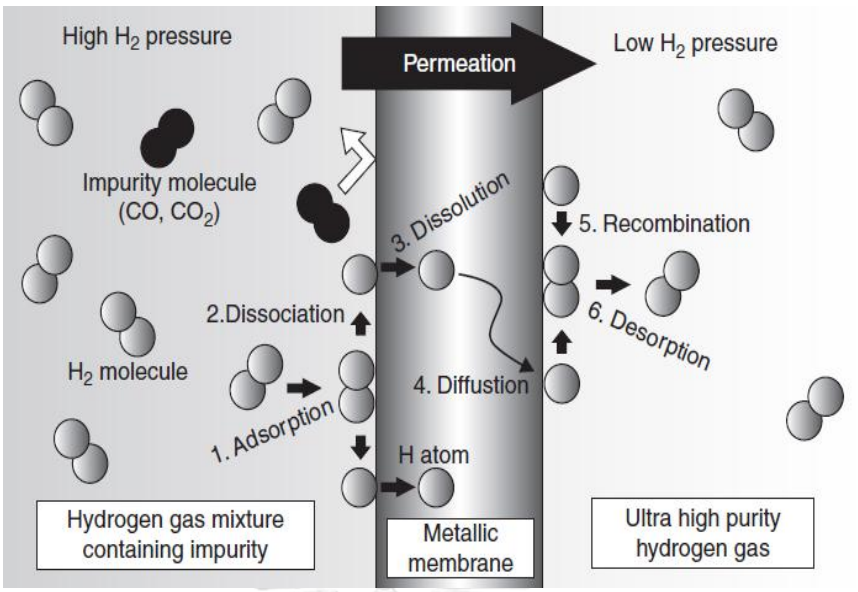

Figure 2. 2 Solution-diffusion mechanism of palladium membrane [13]

For solution–diffusion mechanism, many theories have been proposed to explain the mechanism behind hydrogen diffusion through a metal lattice. Kehr has proposed several different mechanisms for hydrogen diffusion through metal lattices, which depended on the temperature [14].

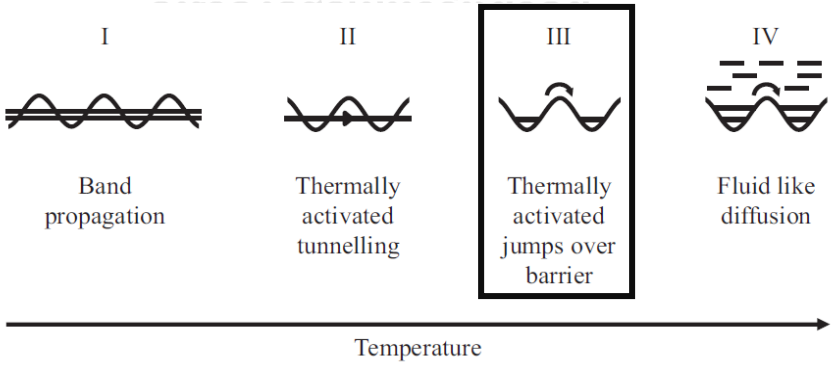

Figure 2. 3 Solution-diffusion mechanism of palladium membrane [14]

The range of operating temperatures for Pd membrane is 300–600 °C. Thus, mechanism hydrogen diffusion in Pd lattice is as shown in Figure 2.3. At Region (III), hydrogen

atoms are modelled as classical particles and are able to execute over-barrier jumps between neighboring interstitial sites [14].

The pressure–composition–isotherms (pci's) is amount of hydrogen and the pressure that absorbed by Pd layer membrane. A schematic phase diagram of palladium hydride is depicted in Figure 2.4. The low hydrogen concentration is at small hydrogen to Pd ratio (H/Pd < 0.1) exothermically dissolved (solid-solution, α–phase) in the Pd. The Pd lattice expands proportional to the hydrogen concentration by approximately 2 to 3 A° per hydrogen atom [15]. At increase hydrogen concentrations in the Pd (H/Pd > 0.1) a strong H–H interaction due to the lattice expansion and the hydride phase (β–phase) nucleates. The coexisting α– and the β– phase can incur a lattice volume expansion more than 10 to 20% of the Pd lattice [12]. Hence, the hydrogen sits within the Pd lattice, internal strains are created which lead to membrane failure. The phenomenon of Pd–H alloy containing the α– and β– phase shows clear evidence of dislocation production which was lose ductility of Pd lattice, a precursor to hydrogen embrittlement [5].

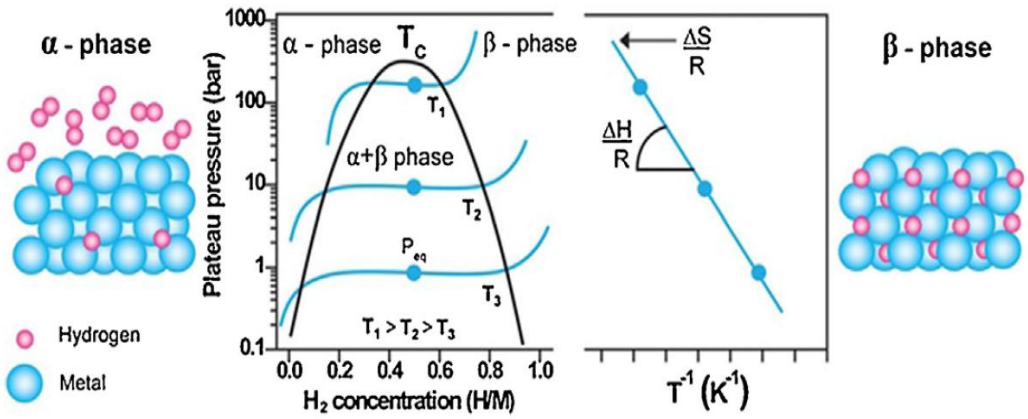

Figure 2. 4 pressure-composition-isotherms for Pd–H [16]

The two–phase region ends in a critical point temperature (T_C), above 300 ºC where only β phase is formed. The equilibrium pressure (P_{eq}) as a function of temperature is related to the changes enthalpy and entropy by the Van't Hoff equation [15].

$$\ln\left(\frac{p_{eq}}{p_{eq}^{0}}\right) = \frac{\Delta H}{R}\cdot\frac{1}{T} - \frac{\Delta S}{R} \qquad 2.1$$

As the entropy change involves to the change from molecular hydrogen gas to dissolved solid hydrogen. The entropy of formation term of metal hydrides leads to a significant heat evolution DQ = T·DS (exothermal reaction) during the hydrogen absorption. The same heat has to be provided to the metal hydride to desorb the hydrogen (endothermal reaction). If the hydrogen desorbs below room temperature this heat can be delivered by the environment. However, if the desorption is carried out above room temperature the necessary heat has to be delivered at the necessary temperature from an external source which may be the combustion of the hydrogen. The enthalpy term characterizes the stability of the metal hydrogen bond [15].

Embrittlement is the weakening of the metal structure caused by the absorption of H atom. The embrittlement of alloy membranes can lead to cracking which allows gases other than H_2 to pass. The effects of embrittlement can be abated through careful selection of operating conditions, the avoidance of pressure pulses and optimizing the support interaction, but the development of embrittlement resistance alloys remains the greatest challenge. The strain in metal to form a microcrack is the initiating mechanism hydrogen embrittlement [17].

According to a database, meatal with face center cubic (FCC) has excellent resistances to hydrogen embrittlement [18]. Pd metal and its FCC alloys are intrinsic more resistant to embrittlement than BCC alloys. Pd can form both α and β hydrides below 298 °C [19] which can result in lattice strains and mechanical failure. Alloying can reduce the critical temperature. Absorption of H can embrittle metals through several mechanisms. Firstly, the α and β phases have different lattice parameters which introduces strain. Secondly, the formation of a second phase within the parent phase (be it a hydride or even a void) reduces the ductility of the parent phase in proportion to the volume fraction of the second phase [20].

The term permeability has several meanings. Permeability is described using Fick's laws of diffusion. The rate limiting step of hydrogen permeation is controlled by the hydrogen diffusion through the bulk Pd layer [21].

$$J = \frac{d}{l} (C_{HP}-C_{LP}) \qquad 2.2$$

where J is the hydrogen flux ($mol/m^2.s$), D is the diffusivity of hydrogen in the Pd membrane (m^2/s^1), l is the thickness of the membrane layer (m), HP and LP are the high and low pressures side of membrane (mol/m^3) and C is the hydrogen concentration [21].

$$C = k\eta \qquad 2.3$$

where k is the concentration constant for hydrogen (mol/m^3), and η is the atomic H/Pd ratio. At very low concentration of hydrogen, η is linearly dependent on the square root of the partial pressure of hydrogen ($C = kp^{1/2}$)

Generally, the relationship for hydrogen concentration in the metal was described by Sievert's law: [22, 23].

$$J = \frac{P}{l} (P_{feed}-P_{perm}) \quad 2.4$$

where J_{H2} is the hydrogen flux (mol/m^2. s), P is the permeability (mol. m/m^2 s. Pa^{-n}), L is the thickness of the membrane layer (m), P^n_{feed} and P^n_{perm} are the partial pressures of the feed side and the permeate side and n is the pressure exponent.

2.2 Alloying

An alloy is a mixture of a metal and another element. Alloying is used in a wide variety of applications such as a combination of metals can be reduced the cost of the material, corrosion resistance or mechanical strength. The physical properties, such as density, reactivity, Young's modulus of an alloy may not differ greatly from the base element, but engineering properties such as tensile strength, ductility, and shear strength may be permanently different from materials. Alloying elements are added to a base metal, to induce hardness, toughness, ductility, or other desired properties. When a molten metal is mixed with another metal, there are two mechanisms that can cause an alloy to form [24]

substitutional alloy: An alloy form, the atoms of the base metal and those of the alloying are of roughly similar size. In most substitution alloys, the constituent elements are quite near one another in the periodic table [24].

interstitial alloy: the interstitial mechanism, one atom is usually much smaller than the other. It can't successfully substitute for the other type of atom in the crystals of the base metal. The smaller atoms become trapped in the spaces between the atoms of the crystal matrix [24].

2.3 PdCu alloy membrane

PdCu alloy membrane has been the most extensively studied of the Pd–based binary alloy membrane because PdCu alloy membrane is resistance to the mechanical, embrittlement, poisoning problems and reduce the cost. Hydrogen embrittlement does not occur to PdCu alloy membrane at low temperature because no hydride phase can from between PdCu alloy and H.

A problem of Pd membrane mentioned above is to keep the membrane above the critical temperature (T_c). This is done by alloying Pd with metals Cu because: [25]

1. Elastic effect: The size of the metal that is replacing the Pd**.** We are known that the Cu atom has a smaller atomic volume than Pd (7.11 and 8.85 cm^3/mol respectively). The more Pd atoms are being replaced by Cu atoms, the less space there is for H atoms in the lattice. With that a higher surrounding H_2 pressure is needed for the system to absorb H.

2. Electronic effect: It considers the interaction of hydrogen electron with the collective band structure of Pd. This effect is based on the fact that Cu, being in the period on the right with respect to the period that contains Pd in the periodic table, brings in an extra d−electron to the band structure. In PdCu the d–band will be filled sooner upon hydrogenation, and the hydrogen solubility will be less than in pure Pd.

Annealing and temperature of alloy illustrates in Figure 2.5, which the relationship between alloy compositions and temperature of PdCu alloy. The following three unique phases can be identified: [26]

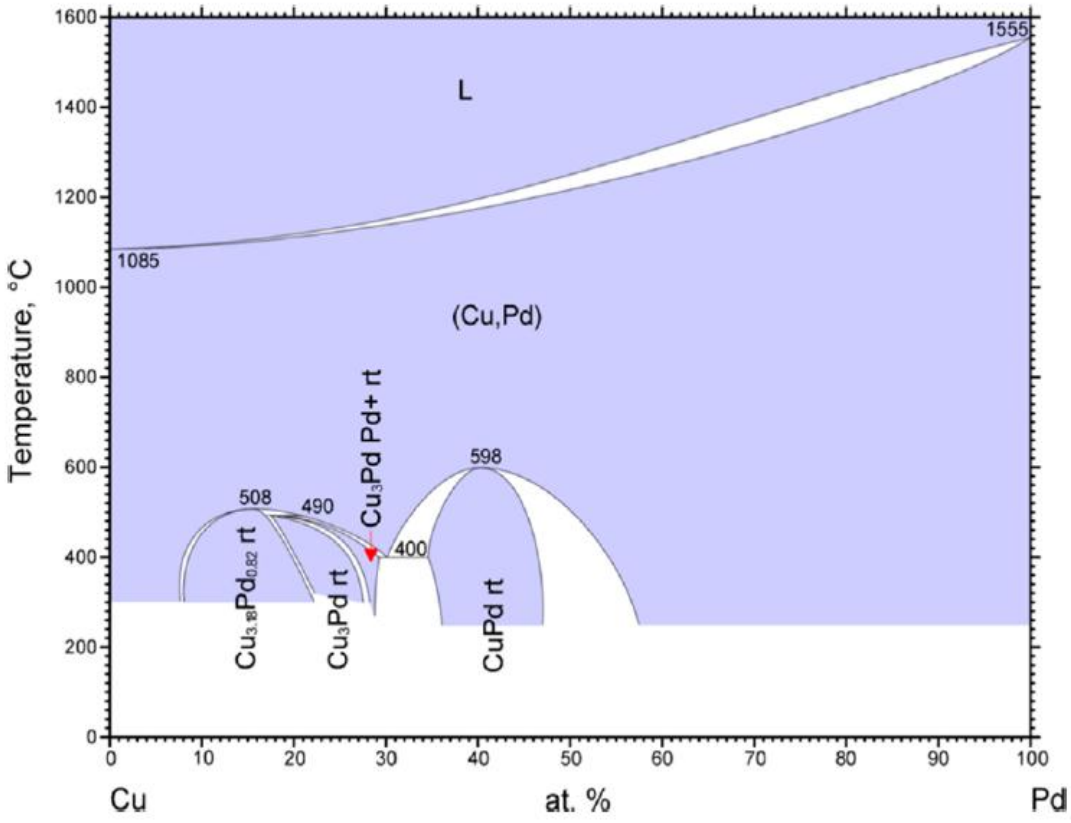

Figure 2. 5 Phase diagram of the PdCu system [27]

(1) the PdCu phase with the B2 (CsCl) bcc-type structure which is stable below 598 °C. The composition ranges from 34 to 47 at% Pd at 400 °C [26].

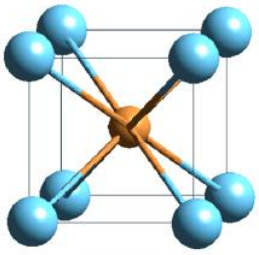

B2 (CsCl)

(2) the $PdCu_3$ phase with the $L1_2$ (AuCu3) fcc-type structure which is stable below 508 °C for alloys with Pd less than ~20 at%. Compositions with 20 to 27 at%

Pd at 400 °C have a distorted $L1_2$ structure with a face-centered tetragonal atomic arrangement,32 while compositions with 27 to 29 at% Pd at 400 °C have another distorted $L1_2$ structure with orthorhombic symmetry below 490 °C [26].

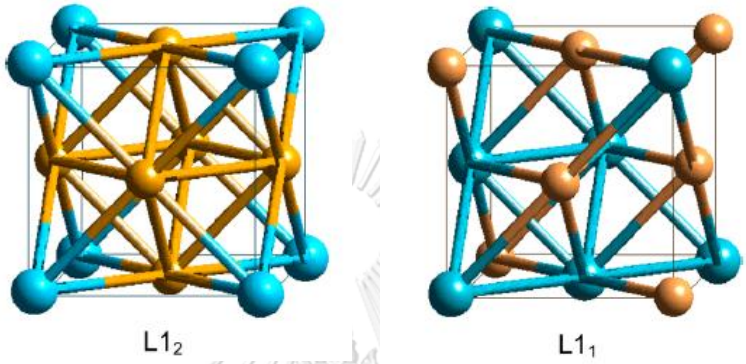

(3) an fcc–type solid solution phase with Cu randomly replaced by Pd can be found when the temperature and composition are outside of the two ranges mentioned above [26].

2.4 Fabrication methods of palladium membranes

In this work, the fabrication of Pd layer alloy membrane was done by using electroless plating (ELP) and electroplating (EP) before the annealing process to form an alloy layer. The concept of these two-deposition technique is described below.

2.4.1 Electroless plating (ELP) of Pd layer membrane

This method is based upon the controlled autocatalytic reaction. The mechanism of electroless plating (ELP) involves the reduction of metallic salt

complexes on the surface of a support material. An activation step was needed to initiate the further reaction. In activation step, the Pd metal seeds on the surface acts as a catalyst for electroless plating that will occur later [28]. The electroless plating method involves seeding a support surface with Pd precursor particles by sensitization and activation, followed by plating of the Pd layer on top of the activated surface as shown in Figure 2.6. The process of sensitization is accomplished by dipping the support into acidic tin ($SnCl_2$) solutions to form $Sn_2(OH)_3Cl$ for Pd particles bonding in the following activation step. This method provides strong advantages such as uniformity of deposits on complex shapes and hardness. Thickness control is not easy due to denposition rate decrease by the time [29].

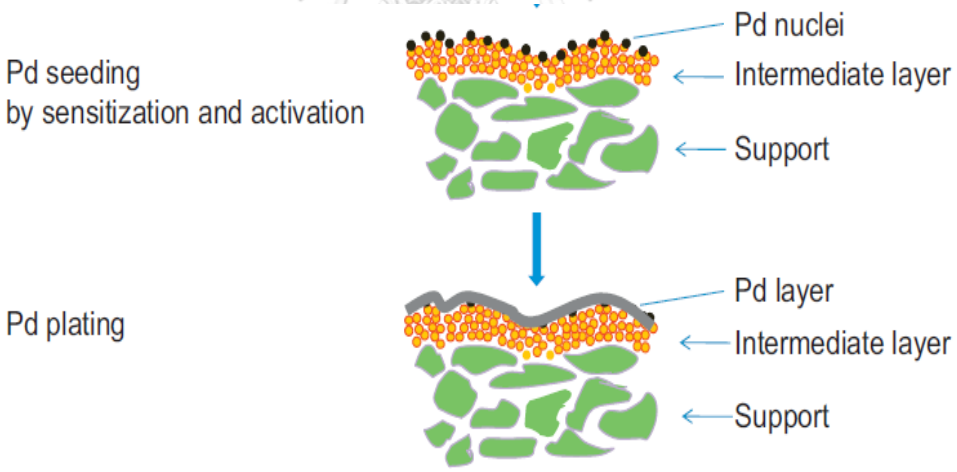

Figure 2. 6 Electroless plating method [19]

2.4.2. Electroplating (EP) of Cu layer

Electroplating (EP) is a liquid-phase electrochemical method in which metal ions are transported by an electric potential and deposited on a substrate, acts as an

anode or cathode. The substrate is placed at a cathode and the positive metallic ions are reduced from metal and deposited on the substrate. Cu layer using EP were described extensively by Shu et al [30]. and Hsieh et al [31]. The advantages of this technique are that it can be conducted with simple equipment and can easily controlling deposition rate depends on plating time, temperature, concentration of solution and current density as shown in Figure 3.6. However, this deposition method is limited to use of conducting support materials such as stainless steel.

2.5 Characterization

2.5.1 X–ray diffraction (XRD)

X–ray diffraction (XRD) technique is used to characterize the physical properties such as crystal structure and composition of materials and thin films. The crystalline of the membrane can identify elements, by comparing diffraction data with a database. The XRD technique is based on the observation of crystalline atoms cause an incident X–ray beam to diffract in different directions. The diffraction occurs in a periodic lattice and the scattered X–rays that were in phase give a constructive interference. This was satisfied for the so-called Bragg's law, defined by:[32, 33].

$$2d\sin\theta = n\lambda \qquad 2.5$$

where λ is the wavelength of the X−rays, d is the interplanar distance between two lattice planes and θ is the angle between the incoming X−rays and the normal to the reflecting lattice plane, as can be seen in Figure2.8.

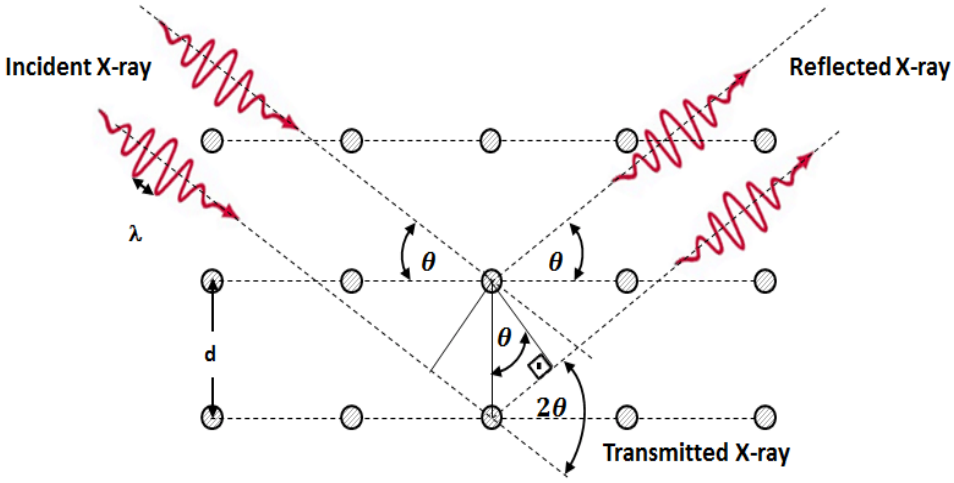

Figure 2. 7 Schematics of the work in principles of Bragg's law XRD [34]

Vegard's law has been used extensively in mineralogy, metallurgy and materials science. The law [35, 36] states that the crystallographic parameters of a continuous substitutional solid solution vary linearly with concentration at constant temperature when the nature of the bonding is similar in the constituent phases. The lattice parameter is controlled by the relative size of the atoms or species exchanged.

The mathematical expression for Vegard's law for a binary solid solution A-B is: [37].

$$a = a_A^0(1-X) + a_B^0 (X_B) \qquad 2.6$$

where $X = X_B$ is the mole fraction of component B and a_A^0 and a_B^0 are the lattice parameters of pure components A and B respectively.

2.5.2 Modern scanning electron microscopy (SEM) and EDS

The scanning electron microscope (SEM) is commonly used for imaging and chemical analysis of the microstructure of the material, i.e. grain sizes, distribution of phases, surface topography and cracks. The energy dispersive X–ray spectroscopy (EDS) analysis is attached to the SEM, for both qualitative and quantitative chemical analysis. An electron beam produced in the electron gun was passed through a series of magnetic lenses and apertures, which provides a focused electron beam. As the beam strikes the sample, the beam electrons interact with the atoms in the sample and a variety of signals is generated see in Figure 2.9. In this work, we used SEM image to study morphology and use x- ray signal to investigate the elemental composition and mapping[38].

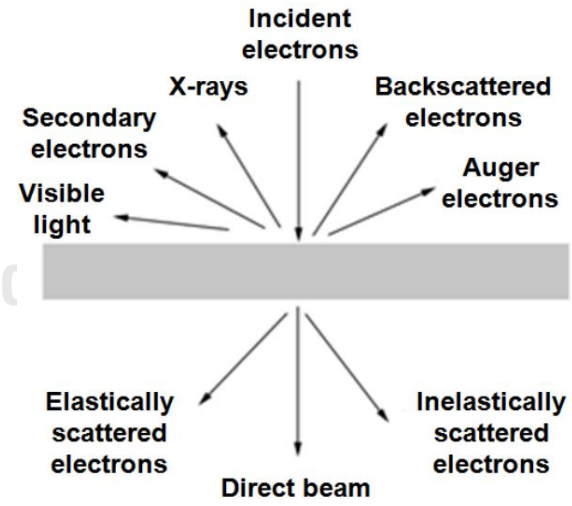

Figure 2. 8 Schematics of the scanning electron microscope [38]

Literature survey

In 2007, Zhang *et al.* [39] fabricated Pd–Cu alloy membranes were prepared by a method called vacuum electroless plating. The hydrogen permeation of Pd–Cu composite membranes with different thicknesses had been studied between 398 K and 753 K. Hydrogen permeance was obtained up to 2.7×10^{-6} mol / (m^2 s Pa) with an ideal selectivity over 1000 at 753 K. The hydrogen permeation exhibited two different activation energies over the temperature range: lower activation energy of about 9.8 kJ/mol above 548 K, while higher activation energy of about 26.4 kJ/mol below 548 K. After permeation tests, we had not observed any structural changes for the membrane Pd–Cu composite membranes under hydrogen atmosphere at the whole temperature range from 423 K to 773 K

In 2009, Decaux *et al.* [40] studied the kinetics of hydrogen permeation of $Pd_{0.47}Cu_{0.53}$ membranes. The permeation mechanism is a multistep process including surface chemisorption of molecular hydrogen, hydrogen diffusion across bulk regions and hydrogen recombination. Diffusion-controlled transport of hydrogen across the membrane is rate-determining. However, the value of the hydrogen diffusion coefficient does not rise exponentially with operating temperature in the 40–400 °C temperature range under investigation, as expected for a thermally activated diffusion process. At temperatures as low as 300 °C, they can be attributed to phase transformation processes induced by temperature and the presence of hydrogen.

In 2010, Pomerantz *et al.* [40] studied the solid-state transformation kinetics of the Pd-Cu alloy from Pd-Cu bilayers for hydrogen separation. Thin layers of Pd and Cu were deposited on porous stainless steel with the electroless deposition method and annealed in hydrogen at 500, 550, and 600 °C. The kinetics of the annealing process was successfully described by the Avrami nucleation. The activation energy for the solid-state transformation was 175 kJ/mol, which was similar to the activation energy of Pd-Cu bulk interdiffusion. The hydrogen permeation tests temperatures at 250, 300 and 350 °C. As a result, the permeance increased because of the higher permeability of the bcc phase.

CHAPTER III

EXPERIMENTAL DETAILS

The experiment was divided in to 4 main parts

3.1 Preparation of stainless steel supports

3.2 PdCu alloy membrane characterization

3.3 Hydrogen permeation flux testing

3.4 Embrittlement test

3.1 Preparation of stainless steel supports

3.1.1 Support cleaning

The non–porous stainless steel (316L SS) sheets were cut into square (1cm × 1 cm and thickness 1 mm), which used to characterize physical properties. The porous stainless steel (316L PSS) was purchased from Mott Metallurgical Corporation. The PSS has a diameter of 0.39 cm and thickness 1mm with the average pore size 0.2 µm. The PSS was used as the support for hydrogen permeation test. Both SS and PSS supports were cleaned with an alkaline solution 1 liter (including 45g $Na_3PO_4.12H_2O$, 65g Na_2CO_3, 45g NaOH and 4ml detergent) at 60 ^oC for 1 hour in an ultrasonic bath. Then, the stainless steel supports were washed three time with deionized water (D.I.) and cleaned in iso-propanol before dried in oven at 120 ^oC for 3 hours, as illustrated in Figure 3.1.

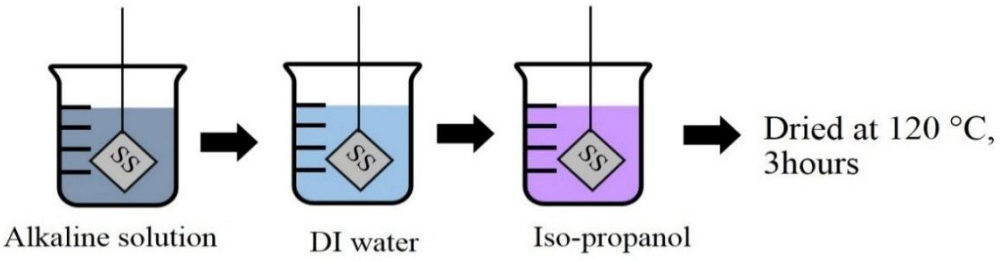

Figure 3. 1 The cleaning step of the support

3.1.2 Activation of supports

Prior the Pd electroless deposition, the stainless steel supports were activated to grow the Pd seeds on surface. The process of activation was done by using sequential immersing of the stainless steel supports into 1 g/l of $SnCl_2$, DI water, 0.1 g/l of $PdCl_2$, 0.01M HCl and DI water respectively. The equation of Pd seeds on the support are showed in equation. 3.1 and 3.2, respectively. After activation process, the surface of support was dark grey color as shown in Figure 3.2. The $SnCl_2$ solution and $PdCl_2$ solution were prepared as follow,

Preparation of $SnCl_2$ solution

In to 1 liter, add approximately 200 mL of DI water, 1 mL of HCl 10M (concentrated 37%) and 1g of $SnCl_2 \cdot 2H_2O$, then shaking to dissolve and adding DI water was filled 1 liter.

Preparation of $PdCl_2$ solution

In to 1 liter, add approximately 200 mL of DI water, 1 mL of HCl 10M (concentrated 37%), 1 g of $PdCl_2$, heating at 60ºC until complete $PdCl_2$ solution and adding DI water was filled 1 liter.

$$2SnCl_2 + 3H_2O \rightarrow 2Sn(OH)_{1.5}Cl_{0.5} + 3HCl \quad (3.1)$$

$$Sn^{2+} + Pd^{2+} \rightarrow Sn^{4+} + Pd^{0} \quad (3.2)$$

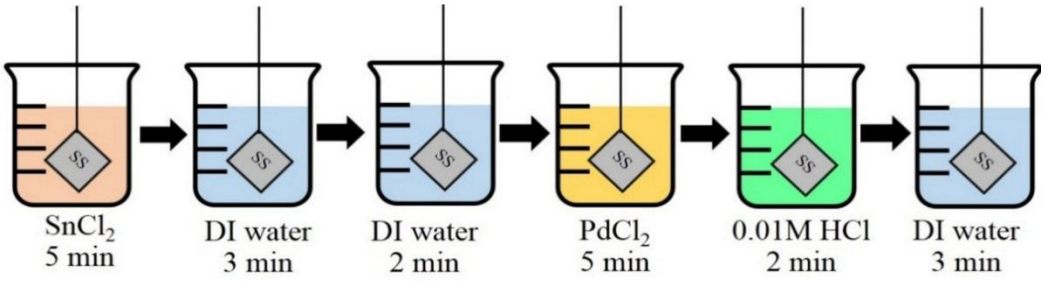

Figure 3. 2 The step for activation process

The morphology of the non-porous stainless steel (316L SS) support was investigated by Scanning electron microscope (SEM). It can be seen from Figure 3.3(a) that the smooth surface of support after cleaning with an alkaline solution. Next step was the activation process of non-porous stainless steel support (Figure 3.3 (b)). It can be seen a large number of seed. For seeding on surface was proposed that tin nuclei were created by decomposing $SnCl_2$ to $Sn(OH)_{1.5}Cl_{0.5}$ with deionized water in equation 3.1. Then, the palladium deposited on the tin layer was the redox reaction in equation 3.2.

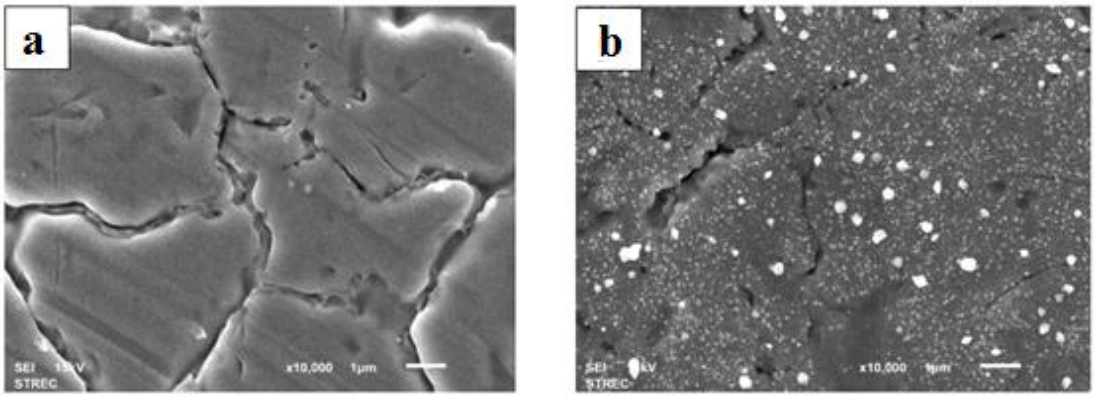

Figure 3. 3 SEM images of the surface morphology of the (a) non-porous 316L stainless steel support and (b) after surface activation

3.1.3 Pd layer deposition

The Pd layer deposition was plated with Pd by electroless plating (ELS) method. The supports were immersed in the Pd plating solution, where the Pd plating solution was at 60 °C. The hydrazine reducing agent was added to immerse of the supports. After plating, the support was dried at 120ºC for about 10 hours. The Pd layer deposition was shown in Figure 3.4. The Pd plating solution and 1 M hydrazine (N_2H_4) solution were prepared as follow,

Preparation of Pd plating solution

In to 1lite, add approximately 200 mL DI water, 4 g of $Pd(NH_3)_4Cl_2 \cdot H_2O$, 198 mL of NH_4OH, 40.1 g of Na_2EDTA and shake gently to dissolve, and make up to 1 liter with DI water.

Preparation of 1M hydrazine (N_2H_4) solution

In to 25 mL, add approximately 10 mL DI water, 0.80 mL N_2H_4 and make up to 25 mL using DI water

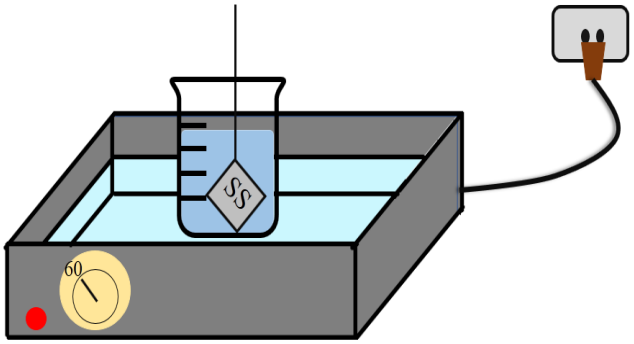

Figure 3. 4 The step for Pd electroless plating in water bath

After support activation process, the deposition of palladium on support by electroless plating method shows surface in Figure 3.5. For Pd eletroless plating occurs redox reaction on the surface of the support and specially around the Pd seed. The primary was reaction by hydrazine with hydroxide ion forming water and nitrogen gas with simultaneous release of electron. The electrons were transferred across the Pd seeds and reduced Pd^{2+} complex into Pd metal. The Pd metal was deposited onto the nuclei resulting in growth. Nitrogen and ammonia gases were evolved as bubbles during the plating process. Pd was deposited on the surface after activation process as following simultaneous reaction:

Anodic Reaction

$$N_2H_4 + 4OH^- \rightarrow N_2 + 4H_2O + 4e^- \quad 3.3$$

Cathodic Reaction

$$Pd[NH_3]_4^{2+} + 4e^- \rightarrow Pd^0 + 8NH_3 \quad 3.4$$

Autocatalytic Reaction

$$Pd[NH_3]_4^{2+} + N_2H_4 + 4OH^- \rightarrow 2\ Pd^0 + N_2 + 4H_2O + 8NH_3 \quad 3.5$$

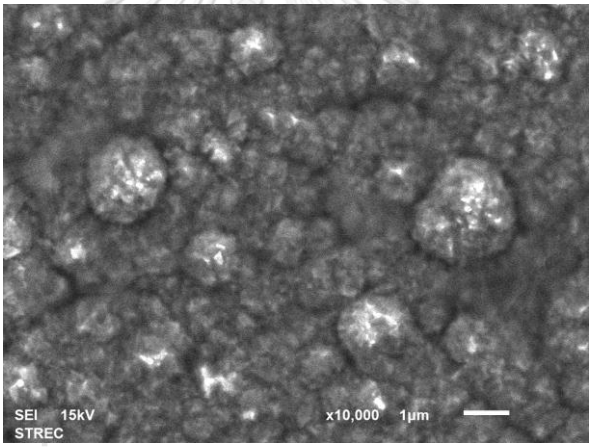

Figure 3. 5 SEM image of Pd surface deposited on non-porous 316L stainless steel support

3.1.4 Cu layer deposition

The Cu layer deposition was plated with Cu by electroplating (EP) method. The Cu layer deposition was plated in 25% $CuSO_4$ plating solution. The distance of 2.0 cm was maintained between the Cu bar and support in 25 mL $CuSO_4$ plating solution. The

plating time was varied 1–6 minutes with operated at 2.0 V. After Cu layer deposition, was immediately in 0.01 M HCl, DI water and ethanol. The Cu layer deposition was shown in Figure 3.6.

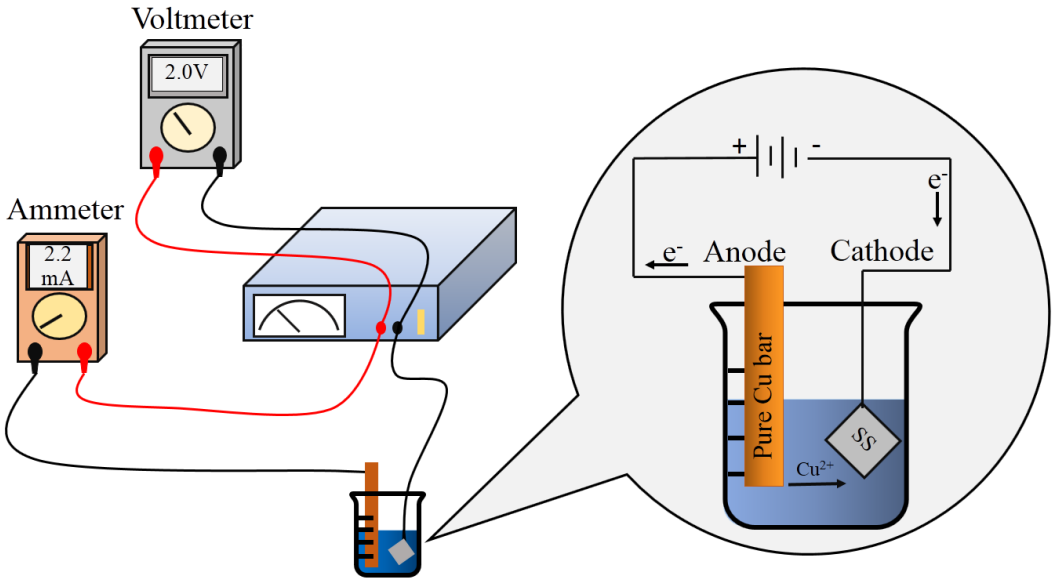

Figure 3. 6 Schematic of Cu electroplating

3.1.5 Alloying process

The Pd-Cu bilayers were then annealed at 500 °C for 24 hours in argon atmosphere.

3.2 PdCu alloy membrane characterization

The surface morphology and thickness of the membranes were performed using JEOL JSM-5800LV scanning electron microscope (SEM). For the cross-sectional, the membranes were prepared by mounting with phenolic resin powder. The cross-

sectional compositions were analyzed by using Oxford energy dispersive x- ray spectroscopy (EDS), attached with SEM.

Phase identification and crystal structure analyses were investigated, using Bruker AXS, D8 Advance x–ray diffractometer (XRD) , equipped with a Cu Kα radiation and operating at 30 kV and 40 mA. The scan rate was 1–2 ° per min and 2θ was in the range of 15–90 °. The XRD results were used to interpret the phase of alloy the membranes.

3.3 Hydrogen permeation flux measurement

The apparatus and setup of the hydrogen permeation measurement were shown in Figure 3.7. To test dense membrane is subjected to helium flux measurement until no more helium flux, indicating that PdCu alloy membrane was dense and covered completely on the porous stainless steel. The PdCu alloy membrane was enclosed in a stainless steel reactor, which was then placed inside the furnace. Then, the PdCu alloy membrane was annealed in a helium gas at rate of 5 °C/min until 150 °C and differential pressure (ΔP) was 0.5 bar. Then, the helium gas was substituted by hydrogen gas. The differential pressure (ΔP) of gas was varied from 0.5-2.5 bar. The furnace temperature was varied from 150-300 °C. Finally, the hydrogen permeation flux was measured by a soap–bubble flow meter. The soap–bubble flow meter was used to determine flow rate by measuring the time required for a gas to move a soap bubble through a specific volume. After testing the membrane with hydrogen, the PdCu alloy membranes were purged with helium gas for 2 hours. The apparatus set up for hydrogen permeation flux measurement was shown in Figure 3.7.

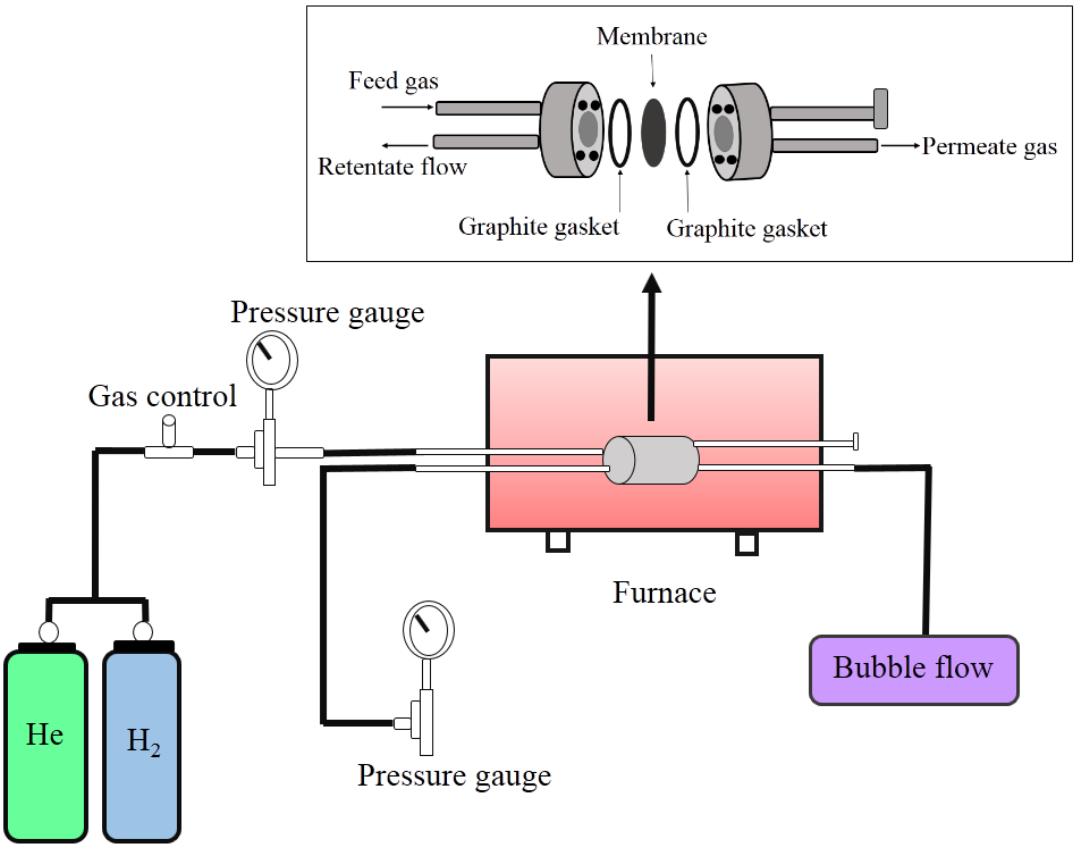

Figure 3. 7 The hydrogen gas permeation set up

3.4 Embrittlement test

As a qualitative measure of the embrittlement was heated in helium gas at a rate of 5 °C/min until 150 °C. Then, the helium was then replaced by hydrogen gas in 2 bar as shown in Figure 3.8. To testing the temperature of membranes were varied from 150 °C – 300 °C. For embrittlement test, the surfaces of membrane were observed before and after hydrogen exposure the temperature range below the critical working temperature of Pd for any signs of cracking by scanning electron microscope.

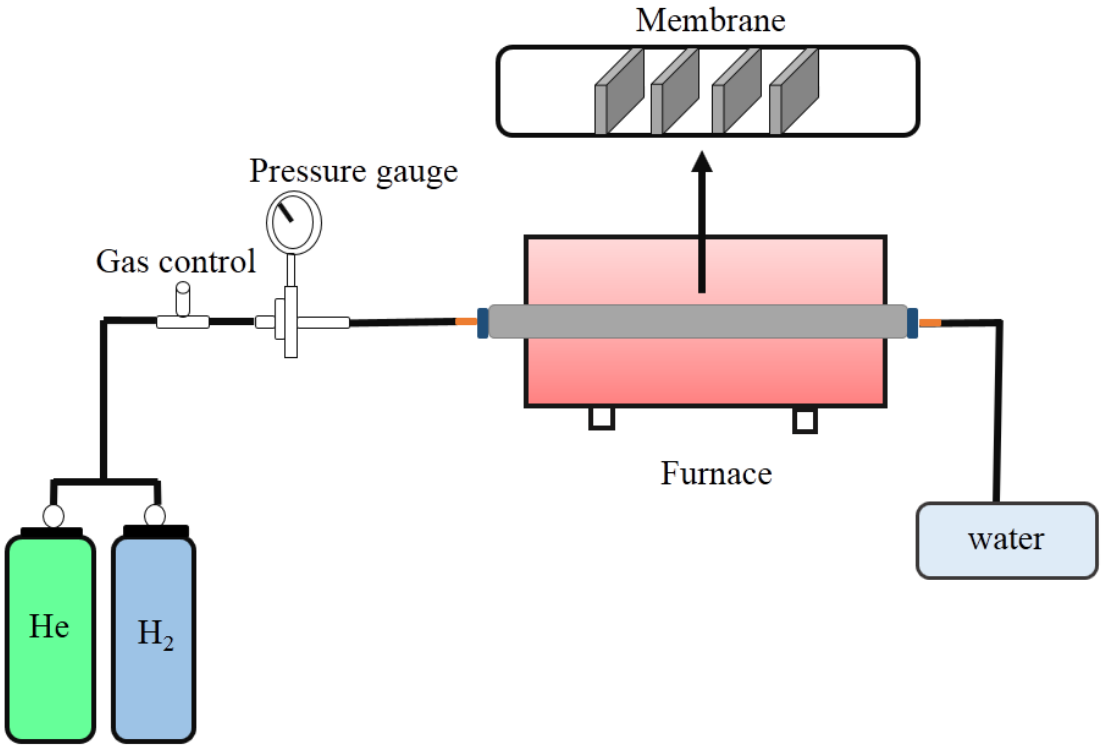

Figure 3. 8 The hydrogen embrittlement set up

CHAPTER IV

RESULTS AND DISCUSSION

The PdCu alloy membranes were prepared by electroless plating and electroplating methods on the supports. The membrane grown on the non-porous stainless steel (316L SS) supports were used to study morphology and physical properties of the membrane. These PdCu alloy membranes were characterized by using SEM-EDS and XRD. The porous stainless steel (316L PSS) supports were used for hydrogen permeation test and embrittlement analysis.

4.1. Deposition rates of Pd and Cu plating

The deposition rate of Pd layer membrane was measured by the thickness of the films, compared with time, using cross-sectional SEM. The deposition rate of Pd layer depends the nuclei process, plating time and plating condition. The thickness of Pd layer membrane increased as the plating time increased. The thickness of Pd layer membrane affects to permeate flux of hydrogen because permeation rate lies on the inverse dependence of the thickness on membrane. The deposition rate of Pd layer was shown in Figure 4.1.

For our eletroless plating growth condition, the deposition rate of Pd layer was found 0.21 µm / minute.

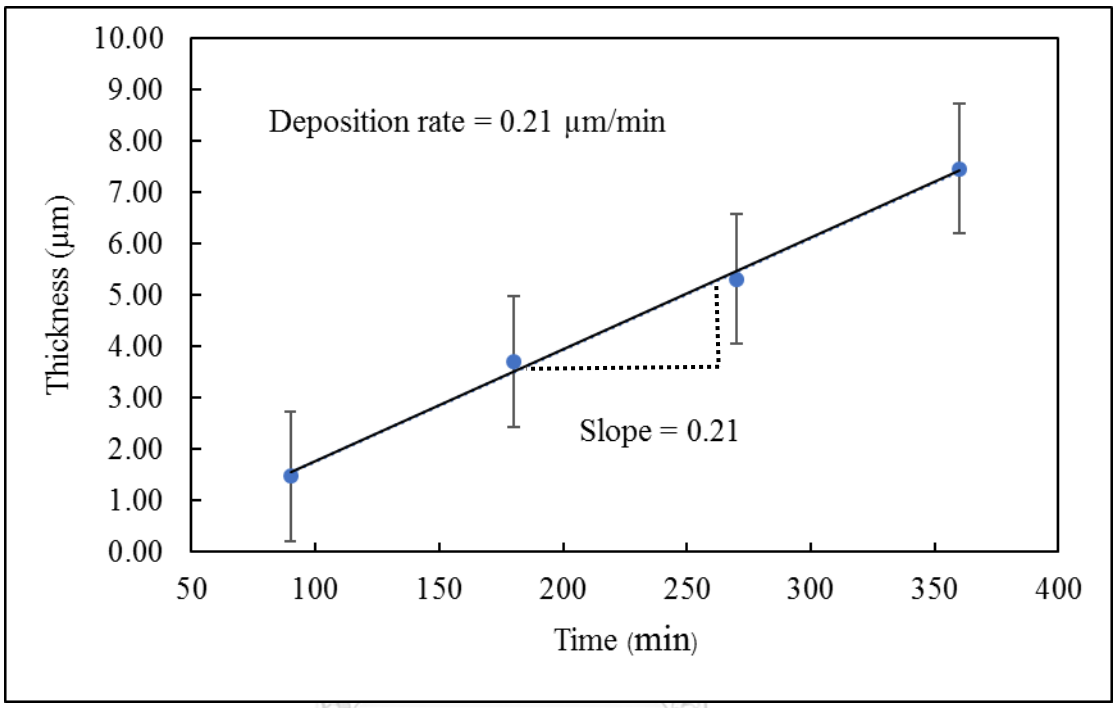

Figure 4. 1 Deposition rate of Pd electrolessplating

Electroplating of Cu layer has been deposited on Pd layer membrane after the electroless plating process. The electroplating method can be a high quality to metal deposition and easy to controlling thickness. The deposition rate of Cu was shown in Figure 4.2.

The deposition rate of Cu layer has 1.93 µm/minute by electroplating method

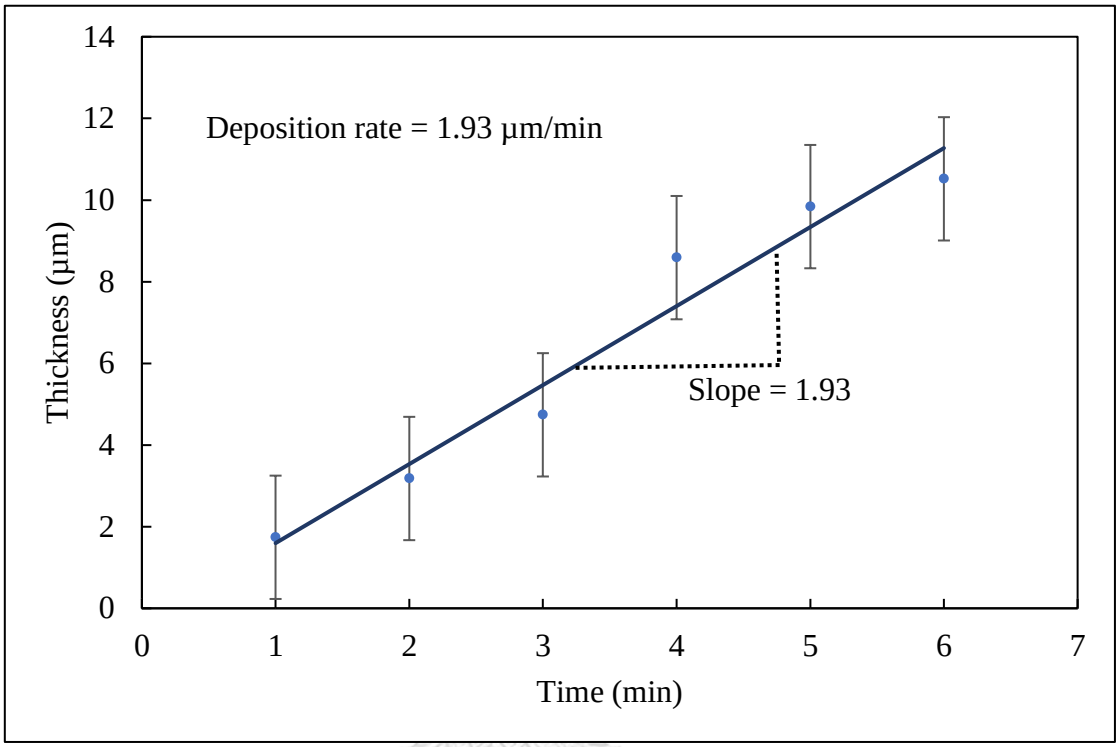

Figure 4. 2 Deposition rate of Cu electroplating

4.2 Alloying of PdCu membrane

The alloying of PdCu membrane was investigated by cross-sectional SEM-EDS elemental mapping. In this work, the annealing temperature of PdCu alloy membrane was at 500 °C to prevent the intermetallic diffusion of the metal elements from the support into Pd layer. The time of thermal annealing was about 24 hours. Before thermal annealing, the micrograph showed clear layer separation of Pd and Cu layers, as shown in Figure 4.3 (a) – 4.10 (a). After annealing, it shows that the Cu atoms have

diffused into Pd layer matrix very quickly due to Cu had a lower Tamman temperature and mobile to thermal vibration at lower temperature than Pd [11]. The PdCu alloys were forms as a single layer, as shown in Figure 4.3(b) – 4.5 (b). However, figure 4.6 (b) – 4.10 (b) indicate the incompleted alloying process for high Cu content sample. There were still some of the remaining copper on the surface, after annealing. This alloying process is relevant for the diffusion in solids, which is significant for microstructural changes that occur during thermal annealing of materials i. e. homogenous of alloys. The diffusion processes are base on Fick's laws, the diffusion coefficient is dependent the concentration gradient of substance and temperature [41]. During the annealing process, Pd and Cu phases have been changed into an alloy form. It affects to a decreased of the driving force as the concentration gradient of pure Cu in the sample lessening and the decreasing of the average diffusion coefficient as the PdCu alloy. Furthermore, Kirkendall has proposed the interdiffusion coefficient, which usually a composition- dependent quantity [42]. Thus, the Pd–Cu interdiffusion coefficient depend on the alloy composition. If more Cu diffused into the Pd, the interdiffusion coefficient would be smaller and the driving force much less [42], which is reasonable to limited amount of Cu.

Pd–Cu bilayer with Cu 1.74 µm (Cu deposition time = 1 min)

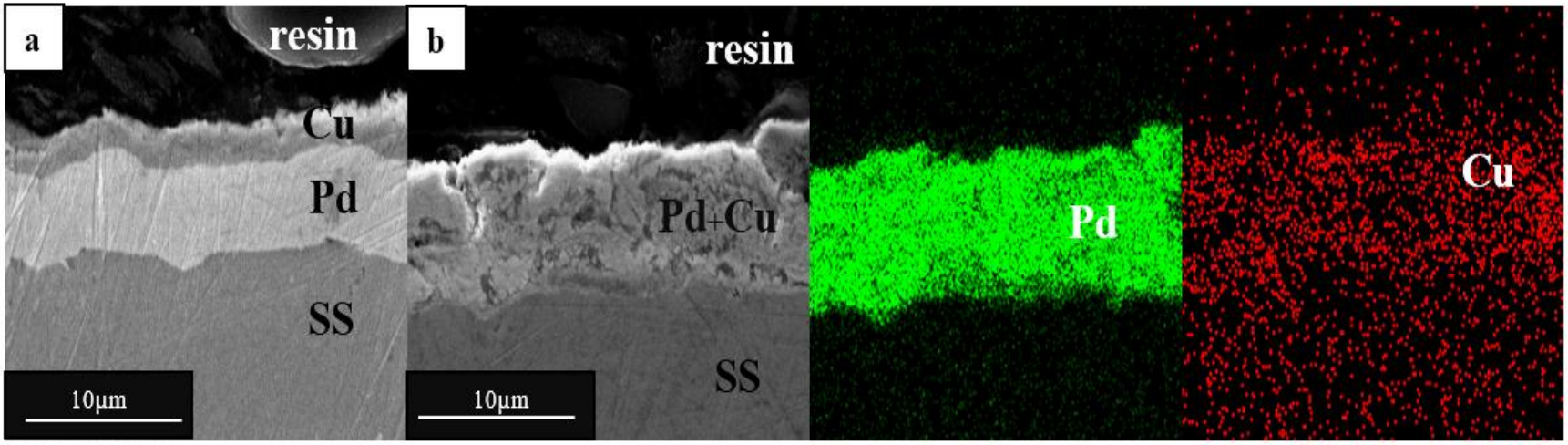

Figure 4.3 Cross–sectional SEM–EDS elemental mapping of Pd–Cu bilayer with Cu 1.74 µm (a) before and (b) after annealing

Pd–Cu bilayer with Cu 2.61 µm (Cu deposition time = 1.5 min)

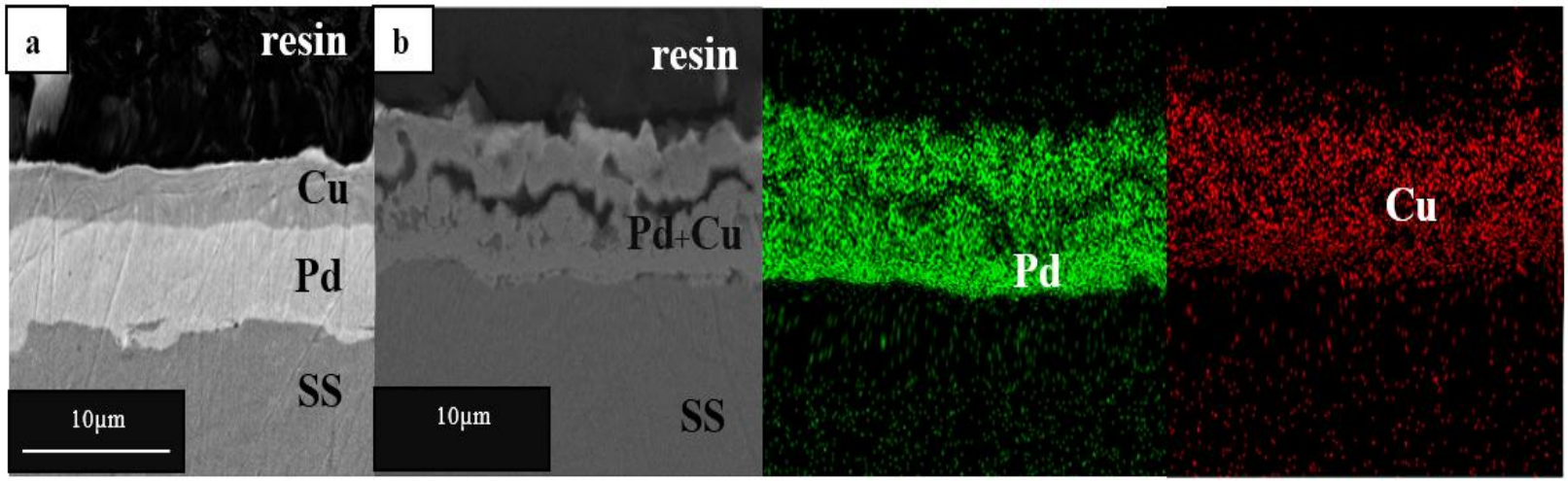

Figure 4.4 Cross–sectional SEM–EDS elemental mapping of Pd–Cu bilayer with Cu 2.61 µm (a) before and (b) after annealing

Pd–Cu bilayer with Cu 3.18 µm (Cu deposition time = 2 min)

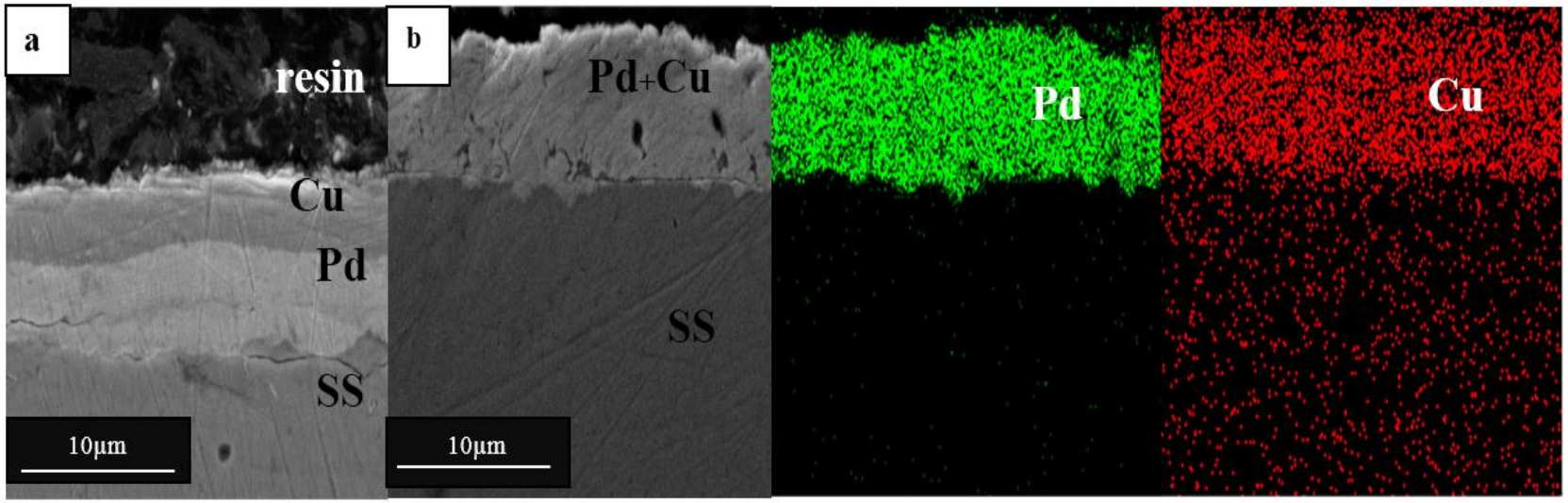

Figure 4.5 Cross–sectional SEM–EDS elemental mapping of Pd–Cu bilayer with Cu 3.18 µm (a) before and (b) after annealing

Pd–Cu bilayer with Cu 3.98 µm (Cu deposition time = 2.5 min)

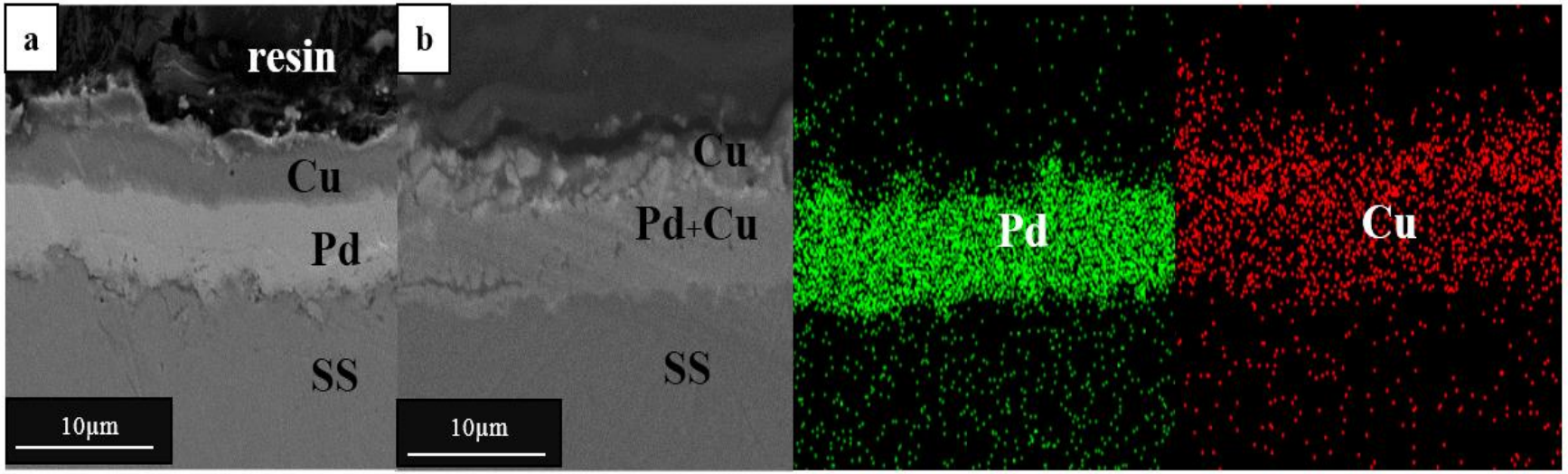

Figure 4.6 Cross–sectional SEM–EDS elemental mapping of Pd–Cu bilayer with Cu 3.98 µm (a) before and (b) after annealing

Pd–Cu bilayer with Cu 4.74 µm (Cu deposition time = 3 min)

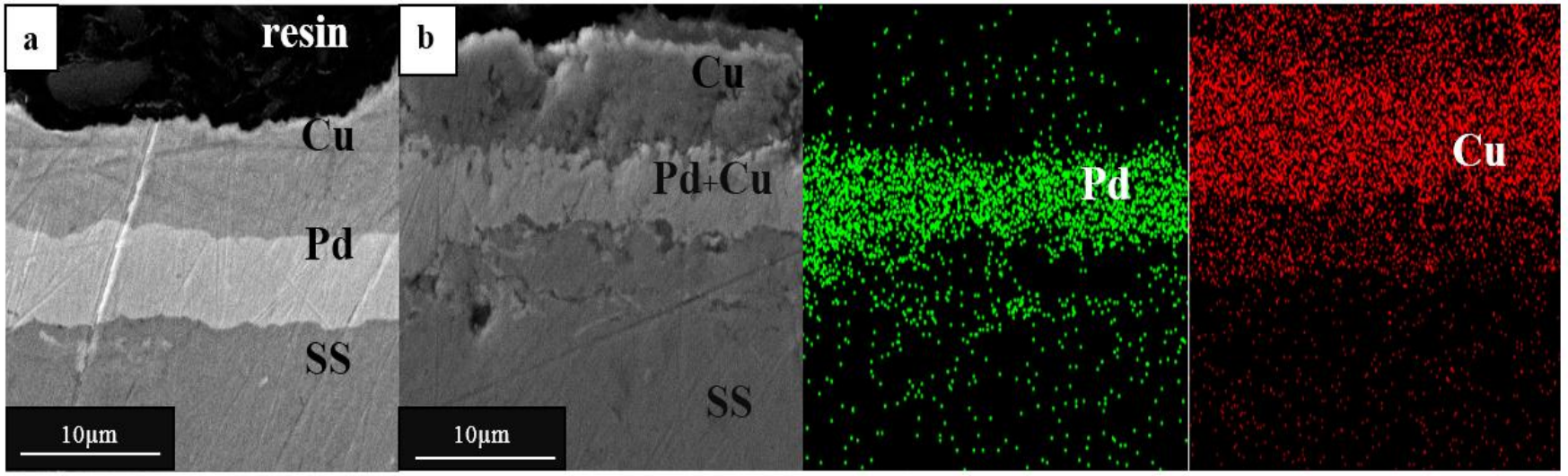

Figure 4.7 Cross–sectional SEM–EDS elemental mapping of Pd–Cu bilayer with Cu 4.74 µm (a) before and (b) after annealing

Pd–Cu bilayer with Cu 8.59 µm (Cu deposition time = 4 min)

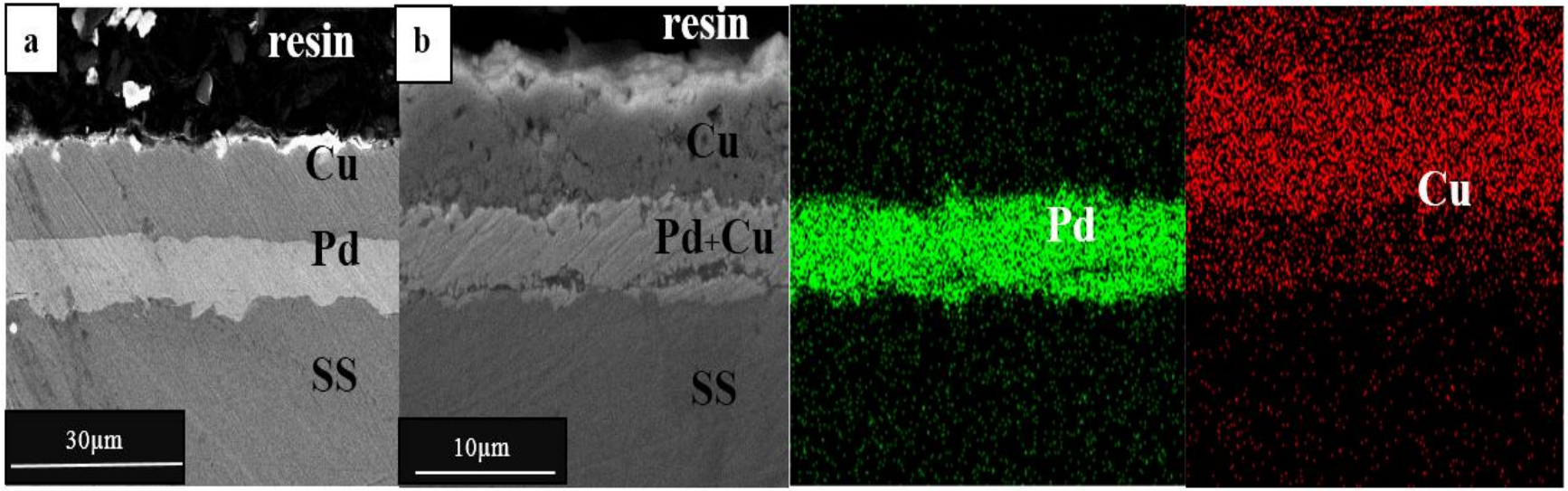

Figure 4.8 Cross–sectional SEM–EDS elemental mapping of Pd–Cu bilayer with Cu 8.59 µm (a) before and (b) after annealing

Pd–Cu bilayer with Cu 9.84 µm (Cu deposition time = 5 min)

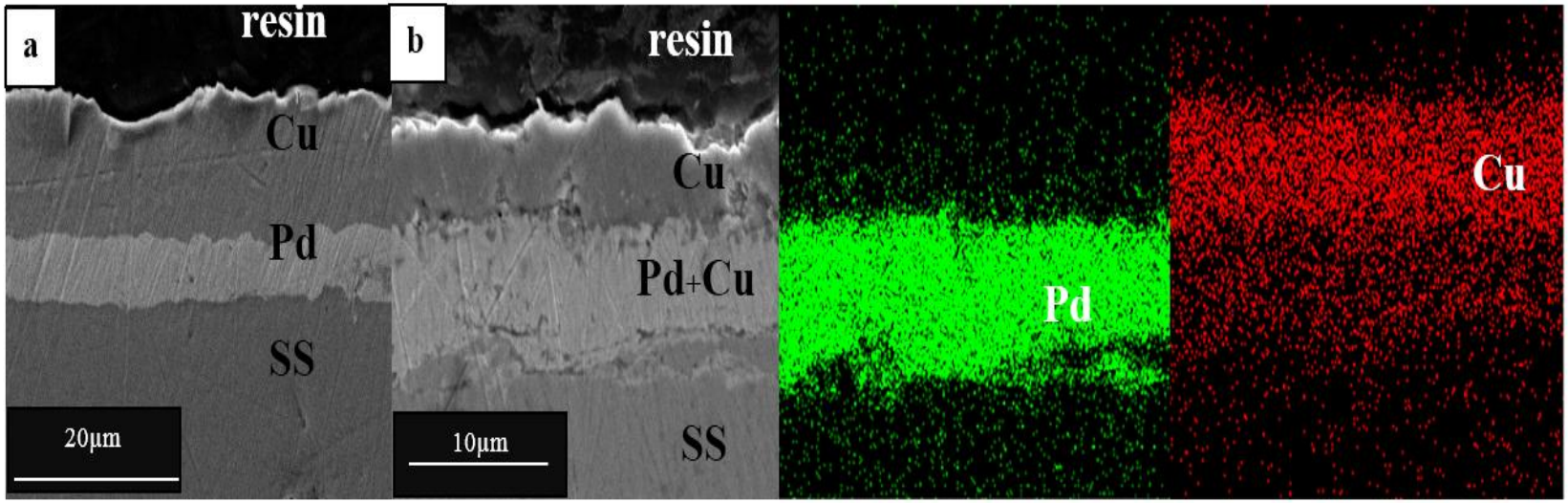

Figure 4.9 Cross–sectional SEM–EDS elemental mapping of Pd–Cu bilayer with Cu 9.84 µm (a) before and (b) after annealing

Pd–Cu bilayer with Cu 10.52 µm (Cu deposition time = 6 min)

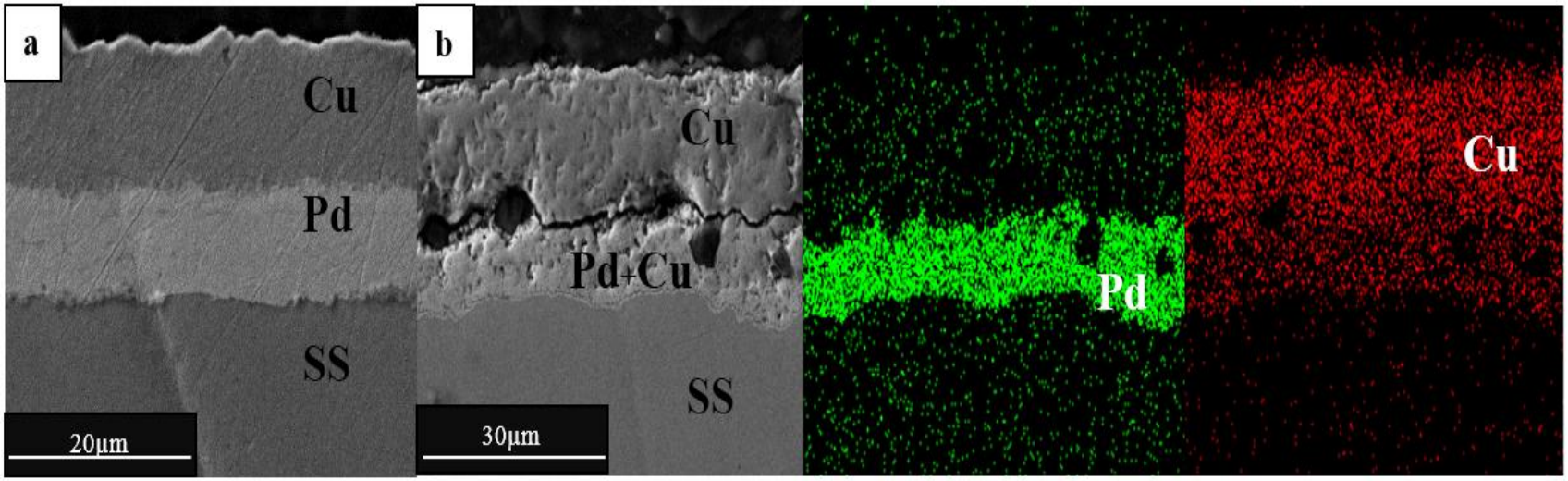

Figure 4.10 Cross–sectional SEM–EDS elemental mapping of Pd–Cu bilayer with Cu 10.52 µm (a) before and (b) after annealing

The result from SEM–EDS elemental mapping showed the element dispersion and homogenous distribution after thermal annealing process. The compositions of PdCu alloy membranes, measured from EDS, were summarized as shown in Table 4.1. The completion of alloy is depended on the deposition Cu amount, resulting in the alloy with different composition.

Table 4. 1 Composition of PdCu alloy membrane

Cu deposition time (min)	Atomic%		Weigh %	
	Pd	Cu	Pd	Cu
1	92.33	7.67	95.27	4.73
1.5	85.17	14.83	90.58	9.42
2	72.82	27.13	81.81	18.19
2.5	70.33	29.67	79.88	20.12
3	67.82	32.18	77.92	22.08
4	64.98	35.02	75.65	24.35
5	63.85	36.16	74.73	25.27
6	62.83	37.17	73.89	26.11

The x–ray diffractograph of the as–deposited Pd-Cu bilayer (unannealed layer) and annealed PdCu alloy in an argon atmosphere was shown in Figure 4.11. The as-deposited of Pd–Cu bilayer illustrates the appearance of each metal peak at different 2θ. After annealing, the atoms of Cu were diffused into Pd matrix and caused the XRD peak shifting, following the alloy composition. Generally, thermal annealing process causes the peak shifts, combination between the peak and new peak appearance. This PdCu alloy exhibited FCC structure with the peaks of PdCu (111), (200), (220) and (311). The result from $Pd_{0.92}Cu_{0.08}$ and $Pd_{0.73}Cu_{0.27}$ alloy are seen to be single peak of alloy. For result from $Pd_{0.70}Cu_{0.30}$, $Pd_{0.68}Cu_{0.32}$, $Pd_{0.65}Cu_{0.35}$, $Pd_{0.64}Cu_{0.36}$, and $Pd_{0.63}Cu_{0.37}$ alloy membranes demonstrated not only the PdCu alloy peak but also the Cu peak for some of alloys. This pure Cu cause copper oxide on membrane. The atomic structure of an alloy is important for the lattice constant parameter. Vegard' law founded that the lattice constant depends on the alloy composition. Pd and Cu were metals with the face-center cubic (f.c.c.) structure. For the face-center cubic (f.c.c.) structures the distance between the atom on the corners of the cube is called the lattice constant ($\boldsymbol{a}$). The general form of PdCu alloy any composition: can be written as Pd_xCu_{1-x}, where x is the number fraction of Pd atom, $0 \leq x \leq 1$ [37]. The Pd has $\boldsymbol{a}$ = 3.890 Å, while Cu has $\boldsymbol{a}$ = 3.614 Å. We used the Bragg's law to calculate the spacing of the Bragg planes d_{hkl}. The lattice constant can be determined by $d_{hkl} = \boldsymbol{a} / \sqrt{h^2 + k^2 + l^2}$. Both calculated values of lattice constant ($\boldsymbol{a}$) of PdCu alloy indicated a decreasing of lattice constant ($\boldsymbol{a}$) of PdCu alloy structure.as Cu content increased. It also means that Cu diffused into the Pd layer by substitution alloy form.

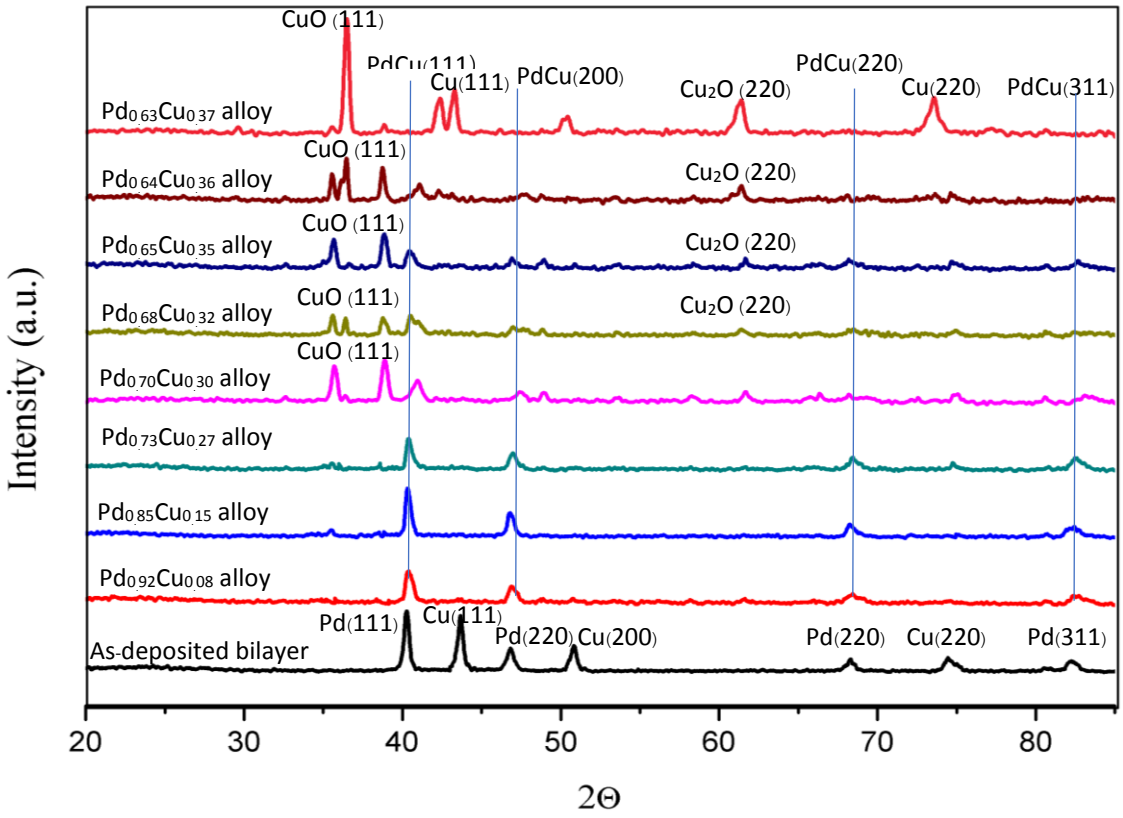

Figure 4. 11 X-ray diffractogram of PdCu alloy

Table 4. 2 Lattice parameter of membrane

Composition %at		Lattice parameter (Å)	
Pd	Cu	Calculation from Vegard' law	Calculated from X-ray diffractogram @Pd(111)
1.00	0.00	3.890	4.288
0.92	0.08	3.869 (↓ 0.54%)	4.276 (↓ 0.28%)
0.73	0.27	3.816 (↓ 1.90%)	4.286 (↓ 0.05%)

4.3 Hydrogen embrittlement

The hydrogen embrittlement tests were performed to examine the extent of embrittling resistance of PdCu alloy membrane, during the use of membranes at 150–300 °C under hydrogen pressure. Normally, hydrogen embrittlement can create the small crack on pure Pd membrane at about temperature 200-300 °C. Figure 4.12 (a–c) show microcracking of Pd layer membrane after exposed to 2 bar of hydrogen atmosphere at 300, 250 and 200 °C, respectively. These cracks can be observed in just a few minutes after operation. Under the same condition applied with the PdCu alloy membranes, the images from optical microscope show membrane surface after hydrogen exposure for 2 hours, as seen from Figure 4.12 (d–i). There was no crack found PdCu alloy membrane surface. This result indicates that PdCu alloy membranes exhibit a good hydrogen embrittlement resistance to operate at the working temperature below the critical temperature of Pd. This benefit of PdCu alloy was caused by the strong interaction between Pd and Cu. With metallic bonds of Pd and Cu, hydrogen can be adsorbed and dissociated only on Pd atoms, but not on copper atoms. This result help to decrease the strain of membrane and increase resistance of hydrogen embrittlement [11].

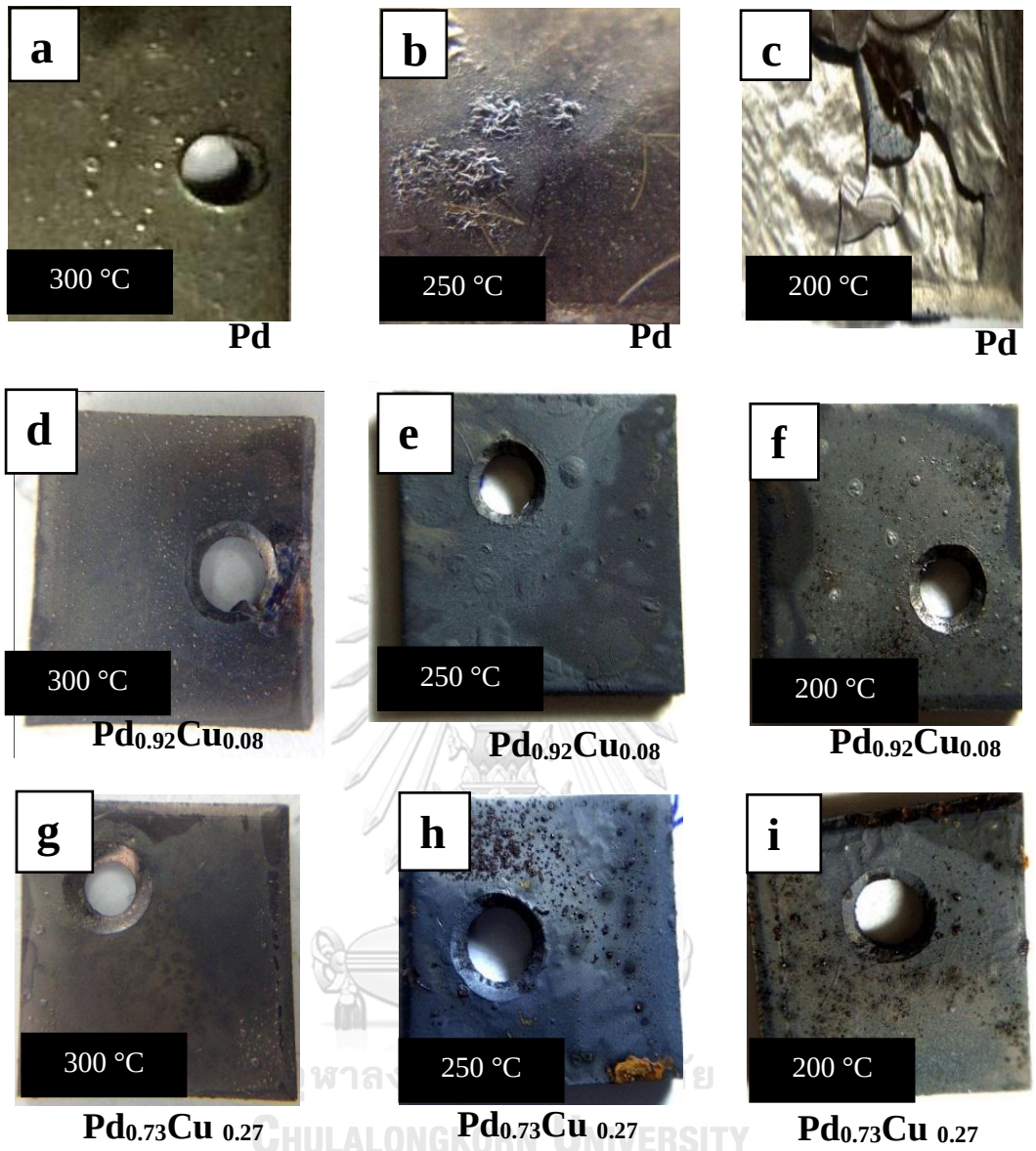

Figure 4. 12 The images from hydrogen embrittlement test at 300, 250 and 200°C for (a–c) Pd, (d–f) $Pd_{0.92}Cu_{0.08}$ and (g–i) $Pd_{0.73}Cu_{0.27}$

4.4 Morphology and composition of PdCu membrane on porous stainless steel (316L) support

The surface morphology of the PdCu alloy membranes surfaces was investigated by using SEM, both before and after deposited on a porous stainless steel support as shown in Figure 4.13 (a) and (b). It can be seen that the pore size of the porous stainless steel is uniformly distributed, as seen in Figure 4.13 (a). After PdCu deposition, the porous surface structure of porous stainless-steel support can induce porosity to the PdCu layer structure, as shown in Figure 4.13 (b).

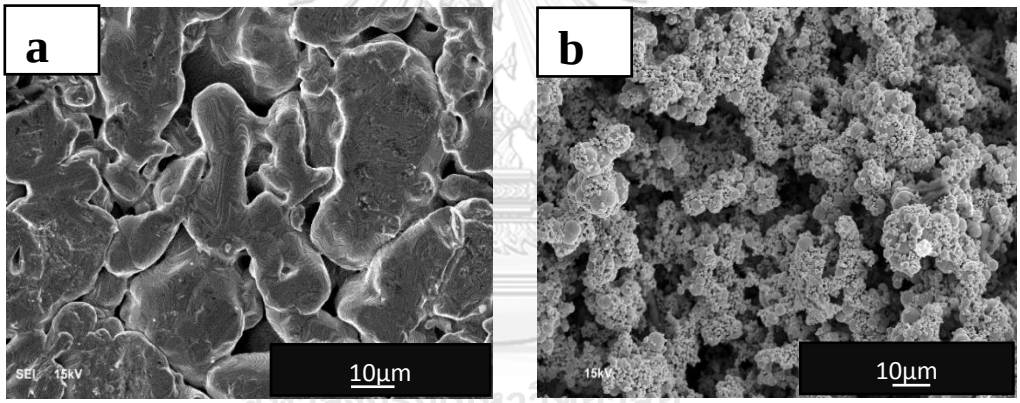

Figure 4. 13 SEM- of the surface morphology of support: before (a) PdCu deposited and (b) after PdCu deposition.

The alloy growth conditions for porous stainless steel supports were the same as those of $Pd_{0.84}Cu_{0.16}$ and $Pd_{0.75}Cu_{0.25}$ on normal stainless steel supports. After alloy annealing, the cross-sectional SEM-EDS (mapping) was performed and the results are shown in Figure 4.14 (a) and 4.15 (a).

The elemental mapping results showed a homogenous and continuous of alloy membrane on the PSS support. Figure 4.14 (b and c) and Figure 4.15 (b and c) show the elemental distribution across the layer for the membranes annealed at 500ºC. From EDS spectra, the average contents of Pd and Cu in the alloy membrane are shown in Table 4.3.

Table 4. 3 Composition of $Pd_{0.84}Cu_{0.16}$ and $Pd_{0.75}Cu_{0.25}$ on porous stainless steel

No.	Weigh %		Atomic%		Thickness (μm)
	Pd	Cu	Pd	Cu	
$Pd_{0.84}Cu_{0.16}$	89.91	10.09	84.19	15.81	38.31
$Pd_{0.75}Cu_{0.25}$	83.56	16.44	75.23	24.77	29.82

$Pd_{0.84}Cu_{0.16}$ alloy membrane

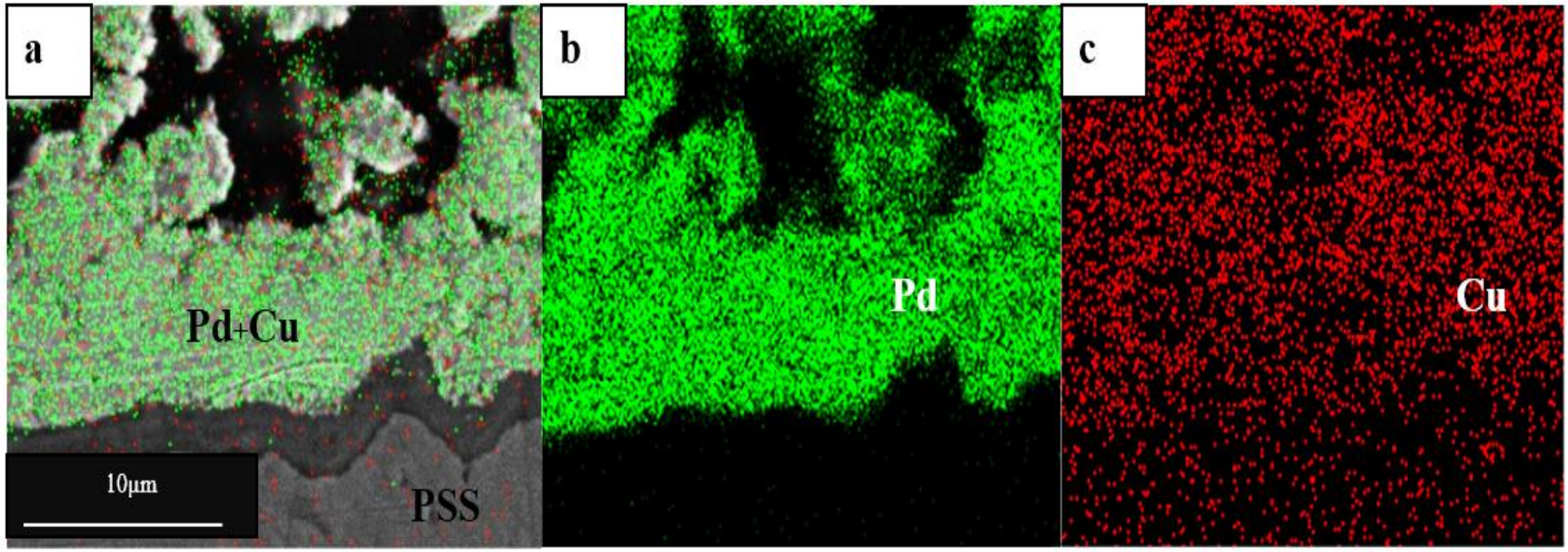

Figure 4.14 Cross-sectional SEM/EDS images of (a) $Pd_{0.84}Cu_{0.16}$ membrane on porous stainless steel, (b) elemental mapping for Pd and (c) elemental mapping for Cu

$Pd_{0.75}Cu_{0.25}$ alloy membrane

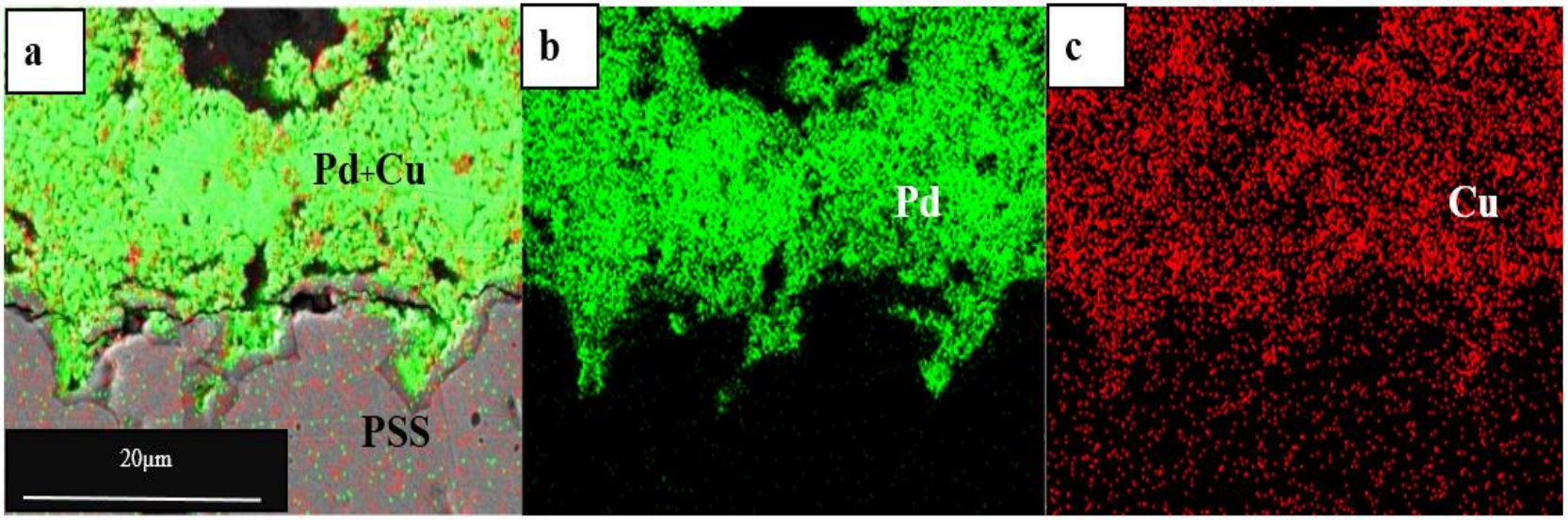

Figure 4.15 Cross-sectional SEM/EDS images of (a) $Pd_{0.75}Cu_{0.25}$ membrane on porous stainless steel, (b) elemental mapping for Pd and (c) elemental mapping for Cu

4.5 Hydrogen permeation test

Generally, the hydrogen permeation flux of membrane follows solution-diffusion mechanism by Sievert's law as equation 2.4. According to solution-diffusion mechanism, hydrogen permeation flux of PdCu alloy membrane consists of adsorption and dissociation of hydrogen molecules, followed by diffusion of hydrogen atoms through the PdCu lattice, recombination of hydrogen atom and desorption of molecular hydrogen. This equation also points out the inverse proportionality of the flux to the membrane thickness. The membrane thickness is also very important; a thinner membrane offers a higher permeability. Thus, the hydrogen permeation flux is directly proportional to the hydrogen partial pressure across the membrane and the hydrogen permeability. In this work, the hydrogen permeation flux of membrane has been at the differential pressures in the range of 0.5-2.5 bar and from temperature 150 °C to 300 °C and hydrogen diffusion of membrane is linearly proportional to the square root of the pressure difference $(P_{feed}^{0.5} - P_{perm}^{0.5}) = \Delta P^{0.5}$ [11]. The hydrogen permeation flux decreases proportional to the thickness of membrane. Figure 4.16 and Figure 4.17 shows a representative relation between hydrogen permeation flux (J) and square root hydrogen pressure ($\Delta P^{0.5}$) for the $Pd_{0.84}Cu_{0.16}$ and $Pd_{0.75}Cu_{0.25}$ alloy membranes. The results show the hydrogen permeation flux has increased with increasing temperature and differential pressure. A higher hydrogen permeation flux is obtained with further thinning of the $Pd_{0.75}Cu_{0.25}$ alloy membrane.

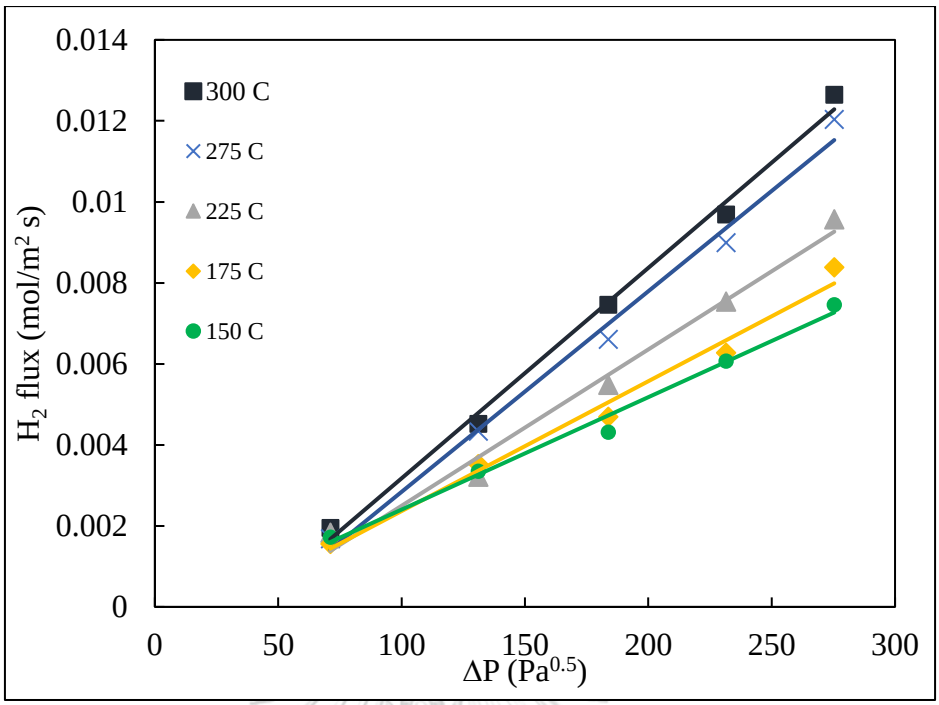

Figure 4. 16 Pressure dependence of hydrogen flux for $Pd_{0.84}Cu_{0.16}$

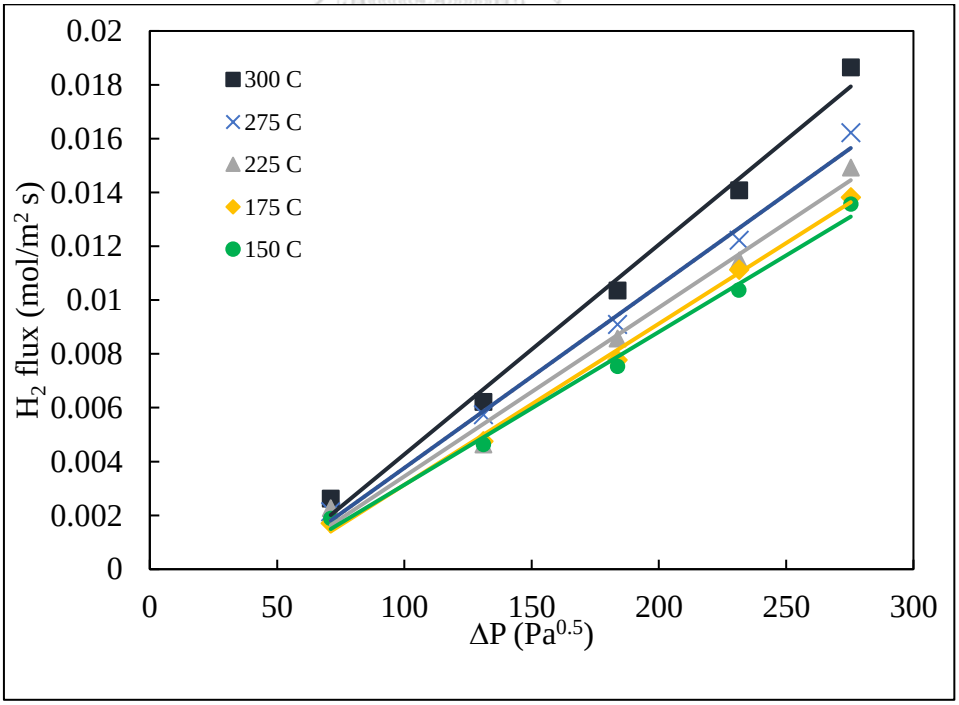

Figure 4. 17 Pressure dependence of hydrogen flux for $Pd_{0.75}Cu_{0.25}$

The permeability is the ability of membrane to be permeable to substance. Therefore, we can calculate the hydrogen permeability of the alloy from the slope of the straight line according to the Sieverts' law, as indicated in Table 4.4. Thus, the permeability value is independent from membrane thickness.

Table 4. 4 Permeability of $Pd_{0.84}Cu_{0.16}$ and $Pd_{0.75}Cu_{0.25}$ on porous stainless steel

No.	Permeability at different temperature (mol.m/m^{2}s Pa^{-n})				
	300 °C	275 °C	225 °C	175 °C	150 °C
$Pd_{0.84}Cu_{0.16}$	2.03×10^{-9}	1.95×10^{-9}	1.53×10^{-9}	1.26×10^{-9}	1.15×10^{-9}
$Pd_{0.75}Cu_{0.25}$	2.33×10^{-9}	2.12×10^{-9}	1.91×10^{-9}	1.82×10^{-9}	1.73×10^{-9}

In addition, as for the influence of temperature on hydrogen permeability. The relationship between the hydrogen permeability and the temperature can be described by the Arrhenius law [11] :

$$P = P_0 \exp\left(-\frac{Ea}{RT}\right) \quad 4.1$$

It can be seen from Arrhenius equation, that there is a dependence of permeability on the operating temperature of the system. The activation energy of membrane can be determined by Arrehenius equation and relating log of permeability obtained from Sievert's law data to the inverse of temperature in Kelvin.

$$\ln P = \ln P_0 \ -\frac{Ea}{RT} \quad 4.2$$

The slope can be used to determine the activation energy, Ea = (slope)(R). Thus, the Arrhenius plots can indicate the activation energy (Ea) for the hydrogen diffusion process in the membrane through the temperature dependence of permeability of membrane, as shown in Figure 4.18. The activation energy for hydrogen diffusion though the membrane was examined from the temperature dependence results of permeability between 150–300 °C. It indicated that the temperature and composition of the membrane would influence to hydrogen flux due to the different in activation energy in hydrogen diffusion processes.

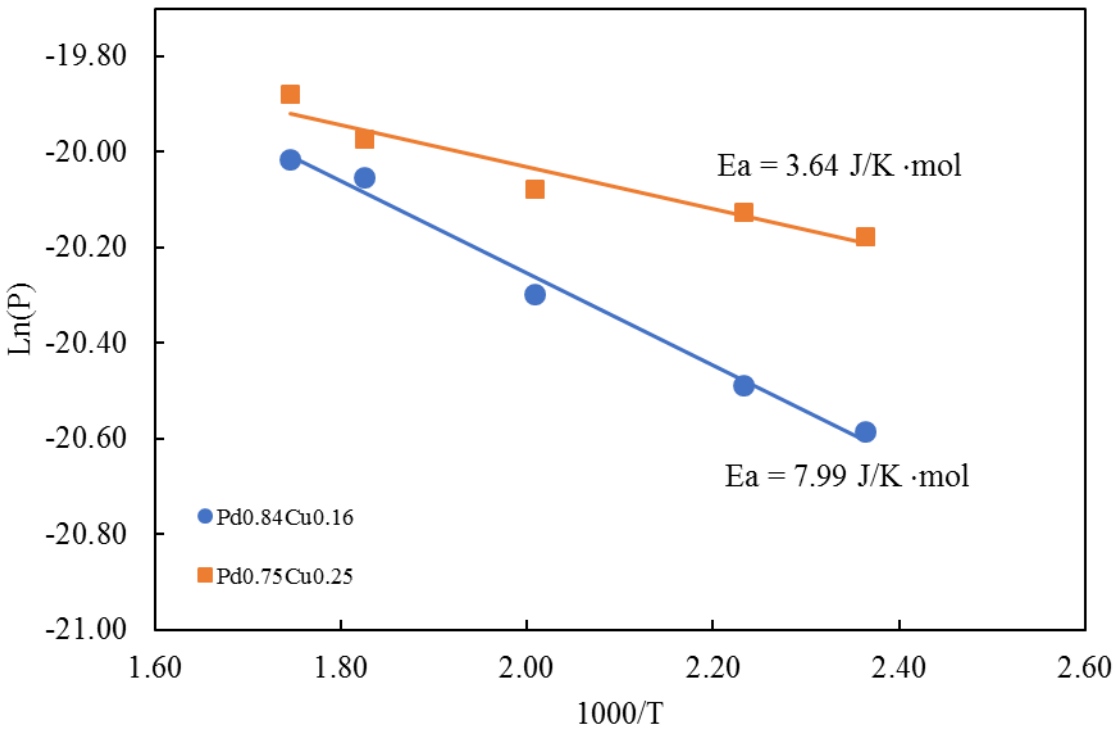

Figure 4. 18 The Arrhenius plots between the hydrogen flux and invert operation temperature of membrane

CHAPTER V

CONCLUSIONS

PdCu alloy membranes for hydrogen separation were successfully prepared by electroless plating and electroplating methods, followed by the annealing to form alloy material. The deposition rate of Pd layer increases with the autocatalytic reaction and the time. The deposition rate of Cu layer increases with the deposition time and current density. Controlling the deposition rate during the electroless plating and electroplating were found to be an important factor to the thickness and composition of membranes. The composition variation of the membranes due to be deposition rate of both materials, were investigated by EDS analysis. We found the limitation of Pd_{1-x} composition to form complete single layer alloy membrane was approximately 75 % at, for our annealing condition. According to the results of XRD and SEM- EDS elemental mapping analysis, it was confirmed that the membranes were attributed of forming a completion alloy. Thicker Cu layer can lead to incompletely alloying process and caused some left over Cu on the surface. For reaction performance of $Pd_{0.84}Cu_{0.16}$ and $Pd_{0.75}Cu_{0.25}$ alloy membrane, both composition can be used for hydrogen separation at the temperature range about 150 °C -300 °C and differential pressure (ΔP) 0.5–2.5 bar. The hydrogen flux increased with an increasing of differential pressure (ΔP) and temperature. The different hydrogen flux throughput of those two membranes can be explained by different hydrogen transport mechanism with different membrane thickness and composition. As shown, a thinner membrane would result in a relatively activation energy, indicating that hydrogen flux was increased. The incorporated Cu

atoms in Pd membrane structure improved the mechanical properties and reduce stress in membrane crystal structure both $Pd_{0.84}Cu_{0.16}$ and $Pd_{0.75}Cu_{0.25}$ alloy membranes can be operated at much lower temperature than the Pd membrane, without any micro-crack due to hydrogen embrittlement.

Future work

- Scale- up of the membrane to larger size and deposition on the tubular support, for industrial applications.

REFERENCES

1. Paglieri, S. and J. Way, *Innovations in palladium membrane research.* Separation and Purification Methods, 2002. **31**(1): p. 1-169.
2. Grashoff, G., C. Pilkington, and C. Corti, *The purification of hydrogen.* Platinum Metals Review, 1983. **27**(4): p. 157-169.
3. Graham, T., *On the absorption and dialytic separation of gases by colloid septa Part I.—Action of a septum of caoutchouc.* Journal of Membrane Science, 1995. **100**(1): p. 27-31.
4. Lewis, F.A., *The palladium/hydrogen system.* 1967.
5. Wise, M., J. Farr, and I. Harris, *X-ray studies of the α/β miscibility gaps of some palladium solid solution-hydrogen systems.* Journal of the Less Common Metals, 1975. **41**(1): p. 115-127.
6. Cotterill, P., *The hydrogen embrittlement of metals.* Progress in materials science, 1961. **9**(4): p. 205-301.
7. Cheng, Y. and K. Yeung, *Palladium–silver composite membranes by electroless plating technique.* Journal of Membrane Science, 1999. **158**(1-2): p. 127-141.
8. Bryden, K.J. and J.Y. Ying, *Nanostructured palladium–iron membranes for hydrogen separation and membrane hydrogenation reactions.* Journal of Membrane Science, 2002. **203**(1-2): p. 29-42.
9. Fort, D., J. Farr, and I. Harris, *A comparison of palladium-silver and palladium-yttrium alloys as hydrogen separation membranes.* Journal of the Less common metals, 1975. **39**(2): p. 293-308.
10. Jun, C.-S. and K.-H. Lee, *Palladium and palladium alloy composite membranes prepared by metal-organic chemical vapor deposition method (cold-wall).* Journal of membrane science, 2000. **176**(1): p. 121-130.
11. Al-Mufachi, N., N. Rees, and R. Steinberger-Wilkens, *Hydrogen selective membranes: a review of palladium-based dense metal membranes.* Renewable and Sustainable Energy Reviews, 2015. **47**: p. 540-551.
12. Koros, W., Y. Ma, and T. Shimidzu, *Terminology for membranes and membrane processes (IUPAC Recommendations 1996).* Pure and Applied Chemistry, 1996. **68**(7): p. 1479-1489.
13. Yukawa, H., T. Nambu, and Y. Matsumoto, *Design of group 5 metal-based alloy membranes with high hydrogen permeability and strong resistance to hydrogen embrittlement*, in *Advances in Hydrogen Production, Storage and Distribution*. 2014, Elsevier. p. 341-367.
14. Kehr, K., *Theory of the diffusion of hydrogen in metals*, in *Hydrogen in metals I*. 1978, Springer. p. 197-226.
15. Züttel, A., *Materials for hydrogen storage.* Materials today, 2003. **6**(9): p. 24-33.
16. Konda, S.K. and A. Chen, *Palladium based nanomaterials for enhanced hydrogen spillover and storage.* Materials Today, 2016. **19**(2): p. 100-108.
17. Dolan, M., *Non-Pd BCC alloy membranes for industrial hydrogen separation.* Journal of Membrane Science, 2010. **362**(1-2): p. 12-28.

18. Yamabe, J., et al., *High-strength copper-based alloy with excellent resistance to hydrogen embrittlement.* International Journal of Hydrogen Energy, 2016. **41**(33): p. 15089-15094.
19. Yun, S. and S.T. Oyama, *Correlations in palladium membranes for hydrogen separation: a review.* Journal of membrane science, 2011. **375**(1-2): p. 28-45.
20. Edelson, B.I. and W. Baldwin Jr, *The effect of second phases on the mechanical properties of alloys*. 1959, CASE INST OF TECH CLEVELAND OH.
21. Steward, S., *Review of hydrogen isotope permeability through materials*. 1983, Lawrence Livermore National Lab.(LLNL), Livermore, CA (United States).
22. Ockwig, N.W. and T.M. Nenoff, *Membranes for hydrogen separation.* Chemical Reviews, 2007. **107**(10): p. 4078-4110.
23. O'Brien, C.P., et al., *The hydrogen permeability of Pd4S.* Journal of membrane science, 2011. **371**(1-2): p. 263-267.
24. Lavakumar, A., *The theory of alloys.*
25. Burch, R. and R. Buss, *Absorption of hydrogen by palladium–copper alloys. Part 1.—Experimental measurements.* Journal of the Chemical Society, Faraday Transactions 1: Physical Chemistry in Condensed Phases, 1975. **71**: p. 913-921.
26. Sha, Y., et al., *DFT Prediction of oxygen reduction reaction on palladium–copper alloy surfaces.* ACS Catalysis, 2014. **4**(4): p. 1189-1197.
27. Hafner, J., *Alloy Phase Diagrams*, in *From Hamiltonians to Phase Diagrams*. 1987, Springer. p. 282-291.
28. Esaka, Y., et al., *Separation of hydrogen-bonding donors in capillary electrophoresis using polyethers as matrix.* Analytical Chemistry, 1994. **66**(15): p. 2441-2445.
29. Ayturk, M.E. and Y.H. Ma, *Electroless Pd and Ag deposition kinetics of the composite Pd and Pd/Ag membranes synthesized from agitated plating baths.* Journal of membrane science, 2009. **330**(1-2): p. 233-245.
30. Shu, J., et al., *Catalytic palladium-based membrane reactors: A review.* The Canadian Journal of Chemical Engineering, 1991. **69**(5): p. 1036-1060.
31. Hsieh, H., *Inorganic membranes for separation and reaction*. Vol. 3. 1996: Elsevier.
32. Askeland, D.R. and P. Webster, *The science and engineering of materials*. Vol. 3. 1996: Springer.
33. Birkholz, M., *Thin film analysis by X-ray scattering*. 2006: John Wiley & Sons.
34. Sowinska, M., *In-operando hard X-ray photoelectron spectroscopy study on the resistive switching physics of HfO2-based RRAM*. 2014, BTU Cottbus-Senftenberg.
35. Smallman, R.E., *Modern physical metallurgy*. 2016: Elsevier.
36. Cullity, B.D., *Elements of X-ray Diffraction.* 2001.
37. Friedel, J., *LX. Deviations from Vegard's law.* The London, Edinburgh, and Dublin Philosophical Magazine and Journal of Science, 1955. **46**(376): p. 514-516.

38. Vernon-Parry, K.D., *Scanning electron microscopy: an introduction.* III-Vs Review, 2000. **13**(4): p. 40-44.
39. Zhang, X., et al., *Hydrogen transport through thin palladium–copper alloy composite membranes at low temperatures.* Thin Solid Films, 2008. **516**(8): p. 1849-1856.
40. Decaux, C., et al., *Time and frequency domain analysis of hydrogen permeation across PdCu metallic membranes for hydrogen purification.* international journal of hydrogen energy, 2010. **35**(10): p. 4883-4892.
41. Sperelakis, N. and J.C. Freedman, *Chapter 8 - Diffusion and Permeability*, in *Cell Physiology Source Book (Fourth Edition)*. 2012, Academic Press: San Diego. p. 113-120.
42. Paul, A., et al., *The Kirkendall effect in multiphase diffusion.* Acta Materialia, 2004. **52**(3): p. 623-630.

APPENDIX

1. Hydrogen flow rate of $Pd_{0.84}Cu_{0.16}$ at various temperature and pressure

Temp (°C)	Test No.	Flow rate (ml/min) at difference pressure (bar)				
		0.5	1	1.5	2	2.5
150	1	0.11	0.25	0.34	0.51	0.61
	2	0.12	0.24	0.34	0.48	0.60
	3	0.11	0.26	0.36	0.48	0.60
	Avg	0.12	0.25	0.35	0.49	0.60
175	1	0.13	0.26	0.37	0.49	0.68
	2	0.14	0.27	0.37	0.50	0.66
	3	0.14	0.27	0.39	0.51	0.68
	Avg	0.14	0.27	0.38	0.50	0.67
225	1	0.16	0.29	0.44	0.63	0.77
	2	0.15	0.28	0.46	0.59	0.76
	3	0.14	0.30	0.43	0.60	0.78
	Avg	0.15	0.28	0.44	0.61	0.77
275	1	0.15	0.34	0.54	0.72	0.96
	2	0.15	0.36	0.55	0.71	0.94
	3	0.17	0.36	0.52	0.73	0.97

	Avg	0.16	0.35	0.53	0.72	0.96
300	1	0.16	0.35	0.62	0.77	1.00
	2	0.16	0.37	0.59	0.76	1.02
	3	0.18	0.36	0.59	0.80	1.02
	Avg	0.17	0.36	0.60	0.78	1.01

2. Hydrogen flow rate of $Pd_{0.75}Cu_{0.25}$ at various temperature and pressure

Temp (°C)	Test No.	Flow rate (ml/min) at difference pressure (bar)				
		0.5	1	1.5	2	2.5
150	1	0.14	0.38	0.62	0.85	1.08
	2	0.13	0.36	0.59	0.82	1.11
	3	0.13	0.37	0.59	0.82	1.08
	Avg	0.14	0.37	0.60	0.83	1.09
175	1	0.14	0.39	0.63	0.89	1.12
	2	0.16	0.37	0.61	0.90	1.10
	3	0.15	0.37	0.62	0.89	1.11
	Avg	0.15	0.38	0.63	0.89	1.11
	1	0.16	0.40	0.67	0.91	1.19

225	2	0.18	0.38	0.69	0.93	1.21
	3	0.18	0.40	0.67	0.91	1.19
	Avg	0.17	0.39	0.68	0.92	1.20
275	1	0.16	0.45	0.74	0.99	1.29
	2	0.19	0.45	0.72	0.96	1.31
	3	0.18	0.47	0.72	0.99	1.31
	Avg	0.18	0.46	0.73	0.98	1.30
300	1	0.21	0.51	0.84	1.14	1.51
	2	0.22	0.48	0.83	1.14	1.48
	3	0.19	0.49	0.82	1.12	1.51
	Avg	0.21	0.50	0.83	1.13	1.50

3. Hydrogen flux of Pd-base membrane

Membrane	Temp (°C)	Hydrogen flux (m^3/m^2h) at $P^{0.5}_{feed} - P^{0.5}_{per}$				
		0.707	1	1.125	1.414	1.581
$Pd_{0.84}Cu_{0.16}$	150	0.06	0.13	0.17	0.24	0.30
	175	0.07	0.14	0.18	0.25	0.34
	225	0.07	0.14	0.22	0.30	0.39

	275	0.08	0.18	0.27	0.36	0.49
	300	0.09	0.18	0.30	0.39	0.51
$Pd_{0.75}Cu_{0.25}$	150	0.07	0.18	0.30	0.41	0.55
	175	0.08	0.19	0.31	0.45	0.58
	225	0.09	0.19	0.35	0.46	0.60
	275	0.09	0.23	0.37	0.50	0.65
	300	0.10	0.25	0.42	0.57	0.75

* Hydrogen flux (m^3/m^2 h) = $\left(\frac{\text{Flow rate of hydrogen (ml/min)}}{\text{Active surface area}}\right) \times 0.6$

Active surface area = 3.14 R^2 (surface area of membrane disk) -3.14 R^2 (surface area of graphite gasket)

= (3.14× 0.65cm× 0.65cm) - (3.14× 0.1cm× 0.1cm)

= 1.195

VITA

Miss Ratchaneekorn Chukiatthaiwas born on April 7, 1993 at Songkla, Thailand. In 2010, she graduated from Hat Yai Ratprachasan School, Songkla . In 2014, she graduated bachelor's degree of Science in Chemistry, Prince of Songkla university, Thailand. She finished master's degree of Science in Petrochemistry and Polymer Science, Chulalongkorn university, Thailand, in 2017.

Presentation:

1. In 2016 Ratchaneekorn Chukiatthai, Supawan Tantayanon, Duangamol Tungasmita, and Sukkaneste Tungasmita, FABRICATION OF PALLADIUM-COPPER ALLOY MEMBRANE FOR HYDROGEN SEPARATION , The 43rd Congress on Science and Technology of Thailand.